

## Global Stability Analysis of the Role of Triple-Bilinear Control Functions for the Treatment of COVID-19 in Nigeria

Bassey Echeng Bassey<sup>1\*</sup>, Igwe O. Ewona<sup>2</sup>

<sup>1</sup>Department of Mathematics, University of Cross River State – (Unicross), Calabar, Nigeria

<sup>2</sup>Department of Physics, University of Cross River State – (Unicross), Calabar, Nigeria

DOI: [10.36347/sjpm.2023.v10i01.002](https://doi.org/10.36347/sjpm.2023.v10i01.002)

| Received: 04.12.2022 | Accepted: 12.01.2023 | Published: 17.01.2023

\*Corresponding author: Bassey Echeng Bassey

Department of Mathematics, University of Cross River State – (Unicross), Calabar, Nigeria

### Abstract

### Original Research Article

**Background:** In this paper, an expanded 10-Dimensional deterministic mathematical dynamic model was formulated that accounted for the role of global stability analysis in the methodological application of dual-bilinear controls with vaccination and impeccable role of adaptive immune response in the control of COVID-19 in Nigeria. In reality, following the introduction of both nonpharmaceutical and pharmacotherapy and the recent availability of vaccines for the control and treatment of the deadly aerosol viral load known as COVID-19, a number of notable scientific investigations on the transmission and treatment dynamics have been conducted but without thoughtful contributions on the combination of these multi-facet control functions that could lead to feasible eradication of the deadly virus.

**Methods:** The model was formulated based expanded 10-Dimensional deterministic dynamic mathematical subpopulations with compartmental interactions investigated using triple-bilinear control functions: bilinear nonpharmaceutical (face-masking and social distancing -  $u_1, u_2$ ), bilinear pharmacotherapies (hydroxychloroquine and azithromycin -  $a_1, a_2$ ) and bilinear immunity controls (adaptive immune effectors and BNT162b2 vaccine -  $m_i, v_i$ ). Experimental Data was collected from University of Calabar Teaching Hospital from the period July, 2022 through September, 2022, as the initial and final time intervals. Apart from fundamental theory of differential equations explored for system mathematical properties, analytical predictions explored classical method of Lyapunov functions with the incorporation of the theory of Volterra-Lyapunov stable matrices for the analysis of the system global stability conditions. **Results:** System mass actions  $\beta_i(\hat{N})$  and the reproduction numbers for both off-treatment  $R_{0(b)}$  and onset-treatment  $R_{0(e)}$  scenarios was for the first time computed with explicit results obtained ( $1.69 \times 10^{-4} \geq \beta_i(\hat{N}) \geq -3.379 \times 10^{-5}$  and  $R_{0(b)} \leq 10.159, R_{0(e)} \leq -3.01$ ). Moreso, off-treatment scenario showed that population extinction was eminent following the unabated exponential spread of the virus after  $t_f \leq 12$  days of asymptomatic infection period. Remarkably, with introduction of triple-bilinear controls, rapid rejuvenation of the susceptible and massive threshold of adaptive immune effectors was achieved at  $t_f \geq 20$  days with resultant high significant reduction to near-zero of viral load and docile COVID-19 environment. **Contributions:** The results of this findings are not only vital in epidemiological studies and applied mathematics but serve a useful source of decision and policy making in the control of COVID-19 and design control for the health sector in Nigeria.

**Keywords:** Triple-bilinear control, adaptive-immune-effector, hypo-hyper-infections, super-spreader, Volterra-Lyapunov-stable, Lyapunov-constant, exponential-spread.

**MSC (2010):** 93A30, 93C15, 34H15, 65L20.

Copyright © 2023 The Author(s): This is an open-access article distributed under the terms of the Creative Commons Attribution 4.0 International License (CC BY-NC 4.0) which permits unrestricted use, distribution, and reproduction in any medium for non-commercial use provided the original author and source are credited.

## 1. INTRODUCTION

Amidst the most spiking deadliest diseases, which by consideration has been assumed to surpass some earlier thought to be the deadliest infectious diseases of the like – human immunodeficiency virus (HIV) and the Ebola virus, is the devastating

coronavirus known commonly as COVID-19. The history of COVID-19 is very much and is still all-over scientific literatures and resource environment world-over. The fact that the current COVID-19, which is an offspring of severe acute respiratory syndrome (SARS-COV-2) and which came into the limelight in 2019 in

the city of Wuhan, China, assume an integral part of the human race, cannot be overemphasized [1, 2].

None-the-less, based on standing literature, symptoms of COVID-19 include the appearance of typical pneumonia marked by cough, fever, headache, dry throat, and subsequent onset acute respiratory syndrome – coronavirus 2 (SARS-COV-2) with life-threatening respiratory failure, [2, 3]. With the transmission of aerosol viral load (COVID-19), cutting across all human races and having the ability of spreading faster in artic-polar regions, the most vulnerable are the elderly (adult of age  $\geq 65$  years). A notable characteristic of COVID-19, which justify its huge existence at asymptomatic infectious stage and which subsequently account for the seeming exponential spread, is the incubation period of 2–14 days [4, 5].

Of note, since the advent of the deadly aerosol viral load, multiple yet epileptic treatment measures, mostly in developing countries have been focused largely on nonpharmaceutical and spatially on clinical testing and diagnosis mechanisms with the use of real-time reverse transcription polymerase chain reaction (RT-PCR) as well as chest computed Tomography (chest CT), (see details [2, 6, 7, 8]. Furthermore, from the evaluation of COVID-19 vaccine efficacy (VE) by the World Health Organization recommended use of laboratory-confirmed outcomes in the form of real-time reverse-transcription polymerase chain reaction (rRT-PCR) for VE evaluation with emphasis specifying 10 days of collection of samples specimens from the onset of infection [9]. Moreso efforts in handling severe cases have led to isolation/quarantization and subsequent hospitalization with the introduction of designated therapeutics. The combination of nonpharmaceutical and designated pharmacotherapies have further enhanced the control of the spread of COVID-19, most probably where control guidelines are strictly adhered [2]. None-the-less, persistent rejuvenation of the virus led to the avocation of an immune boosting mechanism known as vaccines. Clearly, the discovery and introduction of vaccine programs have proven to be significant in the control of deadly disease across the globe. However, enormous cases of reemergence of infection even after access to designated vaccines have equally been reported in many parts of the world. One approach that has the capacity to overcome related infectious diseases is the application of mathematical modeling as a tool for studying the dynamics of infectious diseases and the dynamics of the application of control functions.

For instance, the use of mathematical models was explored to study the combination of Azithromycin with Hydroxyl-chloroquine for Patients Admitted to Intensive Care due to Coronavirus Disease 2019 (COVID-19) – Protocol of Randomized Controlled Trial AZIQUINE-ICU [10]. The results, although at the

trial level, indicated that the patients most likely to benefit from the treatment are those with severe, but with early disease. Curiosity to the possible imperfections in the ability of vaccines lead to the study, “Will an imperfect vaccine curtail the COVID-19 pandemic in the U.S.?” [11]. The results indicated that the prospect of COVID-19 elimination in the US, using the hypothetical vaccine, will be greatly enhanced if the vaccination program is combined with other interventions, such as face mask usage and/or social distancing. Still on the efficacy of the vaccine, research was conducted on the existing and emerging challenges, strategies and prospects of the development and application of COVID-19 vaccines, which yielded significant results [12]. With over 78 vaccines evaluated at clinical trials worldwide, the study was practically on the review of all available COVID-19 vaccines and their underlying mechanisms. The study went further to give summery on progress researches, development and application of COVID-19. Prospects on the crucial role of COVID-19 were equally outlined. Moreso, with the acceptability of COVID-19 vaccines becoming an issue in different quarters, a study on Acceptance of a COVID-19 Vaccine and Its Related Determinants among the General Adult Population in Kuwait, was conducted [13]. The objective of that study was to account and determined the acceptability of COVID-19 vaccine in Kuwait among the adult population. The study explored modified Poisson regression analysis with 95% confidence intervals. Results obtained showed that 53.1% among particpance were willing to be vaccinated against COVID-19 but not without its adverse influencing factors.

Recently, in the United Kingdom, a study aimed to identify risk factors for post-vaccination of SARS-CoV-2 infection users of the COVID Symptom Study app: a prospective, community-based, nested, case-control study was investigated [14]. The studies described the characteristics of post-vaccination illness and came with the results that COVID-19 vaccines show excellent efficacy in clinical trials and effectiveness in real-world data, but some people still become infected with SARS-CoV-2 after vaccination. In that study, it was suggested that any further research on how to enhance the immune response to vaccination in those at higher risk of post-vaccination infection will be highly welcomed. Intensive and related mathematical models on the dynamics of COVID-19 transmission and treatment and/or control measures can as well be found, for example [15-20].

Thus, in view of the above suggestions and the diverging attempts by world body versa-vice classical scientists in diffusing the main route of transmission and control interventions for surging COVID-19 infection, it has been obvious from literature reviews that no clear classical mathematical model, that had considered COVID-19 transmission and treatment dynamics under the methodological combination of

non-pharmaceuticals and multi-therapies in the presence of enhanced adaptive immune system and clinical vaccination programs. Moreso, the dual role of adaptive immune effectors in treatment of COVID-19 has not been incorporated among the aforementioned control measures. Even in the study [38], where simple enrich model was constructed, which accounted for the pharmacological and non-pharmacological policies was investigated, the model was devoid of the dual role of adaptive immune effectors in treatment of COVID-19 pandemic. Therefore, the present proposed investigation considering environment-to-human (hypo) and human-to-human (hyper) transmission outlets, seeks to investigate the interactions evolving around set of varying subpopulations and aerosol viral load (COVID-19) under a designed methodological application of triple-bilinear control functions constituted by: a bilinear nonpharmaceutical (face-masking and social distancing), bilinear pharmacotherapy (hydroxylchloroquine - HCQ and azithromycin – AZT) and bilinear immunity controls (adaptive immune response and *BNT162b2* – vaccine).

Thoughtfully, while Section 1 has been devoted to the introductory aspect, Section 2 depicts the material and methods adopted for the entire investigation. Here, we also highlight the problem statement and derivation of the desired model. In Section 3, we present an explicit investigation of the system mathematical characterization of state- space. The system stability analysis for multiple locally asymptomatic stability as well as its global conditions for COVID-19 is investigated in Section 4. In Section 5, we test the numerical validation of the derived analytical predictions of the study. The evaluation and analysis of the observed outcomes are conducted in Section 6. Constituting the final section 7, are our incisive conclusion and scientific suggestions. The entire study is aimed at providing insight to the possible eradication of the dead infection not only in Nigeria but to the world via enhanced designated triple-bilinear control functions.

## 2. MATERIALS AND METHODS

Here, we shall consider the material and methods of the study as a function of the study problem statement, Derivation of the study mathematical equations and the investigation of the characteristic properties of the model state space.

### 2.1. Problem statement for untreated COVID-19 dynamics

In relation to the present study, two compatible models came to focus. For instance, a COVID-19 transmission dynamic model for the case study of Wuhan in China with nonspecified treatment schedules has been formulated [19]. Facilitated by the results of this finding, an extended version of the model with the introduction of dual-bilinear control functions was

formulated and studied [2]. In-depth review of these models revealed the following limitations:

- i. The model by [19] is by implication peculiar to Wuhan, China, and without the incorporation of treatment functions.
- ii. Death compartment, which was considered as the state variable in the model by [19], is impotent since the deaths do not transmit the virus.
- iii. The non-inclusion of natural source by [19] could lead to abrupt termination of the investigation without desired results.
- iv. Treatment and control measures were not parametrically specified in [19].
- v. The role of the adaptive immune response was not accounted for in both [2, 19] models.
- vi. Immunological time delay lag was not considered for both [2, 19].
- vii. Control function in the model by [2] were vaccine non-inclusive.
- viii. The models [2, 19] were analyzed based on human-to-human transmission mode without accounting for the contributive role of environmental factors.

Thus, in an attempt to overcome the aforementioned limitations, the present investigation using the study [2] as a motivating factor, sought to formulate an improved extended version of COVID-19 model that considers the role of adaptive immunity following the implementation of both the vaccine program and dual-bilinear control functions.

### 2.2. Derivation of model mathematical equations

In view of the aforementioned limitations, we present an expanded 10-Dimensional deterministic COVID-19 mathematical dynamic model, following the incorporation of infectious virus and immune effectors as state variables. The model is studied under triple-bilinear control functions: a bilinear non-pharmaceutical (face-masking and social distancing), bilinear pharmacotherapy (hydroxylchloroquine - HCQ and azithromycin – AZT) and bilinear immunity controls (adaptive immune response and *BNT162b2* – vaccine). Furthermore, in addition to the existing assumptions of the model [2], the uncertainties of the present study are limited by the following basic assumptions.

#### Assumption 1

- i. Only severely infectious die due to virus i.e.  $\alpha_{i=1,\dots,5} \geq 0$ .
- ii. Transmission dynamics revolve within environment-to-human and human-to-human with  $\beta_{i=1,\dots,5} > 0$ .
- iii. Immunity delay lag  $e^{-\alpha_i \alpha_i} > 0$ .
- iv. Only the susceptible and isolated receive vaccine i.e.,  $\nu_{i=1,2} > 0$ .

- v. Immune effectors exhibit a dual role – as state variable  $E_i$  and as control function  $m_{i=1,2}$ .

Now, suppose the formulation and analysis of the study is based on the following subpopulations: susceptible population who are not COVID-19 positive but may be infected if completely exposed  $S_p(t)$ , the exposed class  $X_p(t)$ , the unaware asymptomatic infectious population  $A_u(t)$ , subpopulation of COVID-

19 aware infectives  $I_a(t)$ , isolated infectious subpopulation  $I_s(t)$ , proportion of super-spreaders  $S_s(t)$ , proportion of hospitalized infectives  $H_i(t)$ , recovered population  $R_p(t)$ , the immune effectors  $E_i(t)$  and  $C_v(t)$  representing the concentration of infectious coronavirus. Then, for the population with volume measure in  $cells/ml^3$ , the differential epidemiological dynamic equation for the present study are derived as:

$$\begin{aligned} \frac{dS_p}{dt} &= b_p + m_1 E_i \sigma_1 X_p + \sigma_2 R_p - \beta_i(\hat{N}) S_p - (\mu + v_1) S_p, \\ \frac{dX_p}{dt} &= \beta_i(\hat{N}) S_p + m_2 E_i \sigma_3 A_u - (1 - u_1) \lambda X_p - (\mu + m_1 \sigma_1 E_i) X_p, \\ \frac{dA_u}{dt} &= (1 - u_1) \lambda X_p - [(1 - u_2) k \theta + (1 - a_1)(1 - a_2) \varphi_1 + \varphi_2] e^{-\omega_1 \alpha_1} A_u - (\mu + m_2 E_i \sigma_3) A_u, \\ \frac{dI_a}{dt} &= (1 - u_2) k \theta e^{-\omega_1 \alpha_1} A_u - [(1 - a_1)(1 - a_2) \rho_2 + a_1 \tau_1 \rho_1 + (1 - \rho_1 - \rho_2)] I_a - \alpha_2 I_a, \\ \frac{dI_s}{dt} &= a_1 \tau_1 \rho_1 I_a + a_1 \tau_2 \gamma_s S_s - [(1 - a_1)(1 - a_2) \delta_h] I_s - (\alpha_4 + v_2 \eta_2) I_s, \dots \dots \dots (1) \\ \frac{dS_s}{dt} &= \varphi_2 e^{-\omega_1 \alpha_1} A_u + (1 - \rho_1 - \rho_2) I_a - a_1 \tau_2 \gamma_s S_s - [(1 - \rho_1 - \rho_2) \varphi_2] e^{-\omega_2 \alpha_1} S_s - (\alpha_5 + \eta_3) S_s, \\ \frac{dH_i}{dt} &= \begin{cases} (1 - a_1)(1 - a_2) \varphi_1 e^{-\omega_1 \alpha_1} A_u + (1 - a_1)(1 - a_2) [\rho_2 I_a + \delta_h I_s] \\ - [(1 - a_1)(1 - a_2) [\varphi_1 + \rho_2 + \delta_h]] e^{-\omega_2 \alpha_1} H_i - (\alpha_3 + \eta_1) H_i \end{cases}, \\ \frac{dC_v}{dt} &= s \left( 1 - \frac{C_v}{Q} \right) C_v + (1 - \rho_1 - \rho_2) \varphi_2 e^{-\omega_2 \alpha_1} S_s + [(1 - a_1)(1 - a_2) [\varphi_1 + \rho_2 + \delta_h]] e^{-\omega_2 \alpha_1} H_i - \mu_v C_v, \\ \frac{dR_p}{dt} &= \eta_1 H_i + v_2 \eta_2 I_s + \eta_3 S_s + v_1 S_p - (\mu + \sigma_2) R_p, \\ \frac{dE_i}{dt} &= \zeta_E + \frac{b_E(S_s + H_i)}{(S_s + H_i) + C_b} E_i - \frac{d_E(S_s + H_i)}{(S_s + H_i) + C_d} E_i - \mu_E E_i, \end{aligned}$$

with initial conditions  $S_p(t_0) > 0, X_p(t_0) > 0, A_u(t_0) > 0, I_a(t_0) > 0, I_s(t_0) > 0, S_s(t_0) > 0, H_i(t_0) > 0, R_p(t_0) > 0, C_v(t_0) > 0, E_i(t_0) > 0$  for all  $t = t_0$  and having system mass action  $\beta_i(\hat{N}_i)$  defined by

$$\beta_i(\hat{N}) = (1 - u_1 - u_2) \left[ \frac{\varphi_{C_v}}{Q + C_v} \left( \sum_{i=1}^5 \beta_i c_i(\hat{N}_i) \right) \right], \quad i = 1, \dots, 5 \dots \dots \dots (2)$$

where  $\hat{N}_i = (X_p + A_u + I_a + S_s + H_i)$ .

Of note, system (1) represents an expanded environmental-to-human (*hypo infectious*) and human-to-human (*hyper-infectious*) untreated COVID-19 dynamic model, provided control functions  $c_f$  is such that  $c_f \equiv (u_i, a_i, m_i, v_i) = 0, \quad i = 1, 2$  for all  $\beta_i(\hat{N}) > 0, i = 1, \dots, 5$ . Critically, the right-hand side of system (1) is continuous within time interval  $[t_0, t_f]$ , bounded by sum of control functions and is described by a number of nonlinearities terms, [22, 39, 40].

In explicit terms, we present the description of system (1) as follows: in the first equation, the first three terms  $b_p, m_1 E_i \sigma_1 X_p, \sigma_2 R_p$  present source rates for the susceptible population. The rate at which the susceptible becomes infected following a varying range of interactions is known as system **mass action** and is depicted by  $-\beta_i(\hat{N}) S_p$ . The last term  $-(\mu + v_1) S_p$  represent the natural clearance rate and the proportion of susceptible that are successfully vaccinated. In the

second equation, the source rate of the exposed population is routed to the rate of mass action denoted by  $\beta_1(\hat{N})S_p$  and the proportion of reversed unaware infectives due to efficacy of adaptive immune effectors  $m_2E_i\sigma_3A_u$ . The proportion of exposed to face mask that progresses to asymptomatic infectious is given by  $-(1-u_1)\lambda X_p$ , while the last term  $-(\mu+m_1\sigma_1)X_p$  define clearance rate due to natural death and activity of the immune response.

In the third equation, the first term  $(1-u_1)\lambda X_p$ , represent the proportion of exposed class under face-masking that becomes unaware asymptomatic infectious. The second term  $-(1-u_2)k\theta+(1-a_1)(1-a_2)\varphi_1+\varphi_2]e^{-\omega_1\alpha_1}A_u$  depicts the rates at which the unaware asymptomatic progresses to become aware, infective, get hospitalized, and super spreaders, noting the biological implication of immune time delay lag  $e^{-\omega_1\alpha_1}$ . Clearance in this compartment is due to natural death rate and immune effectors denoted by  $-(\mu+m_2E_i\sigma_3)A_u$ . The fourth equation describes the aware infectives with source rate given by  $(1-u_2)k\theta e^{-\omega_1\alpha_1}A_u$ . The progression rate of this compartment to isolation, super spreaders, and hospitalization is given by  $-(1-a_1)(1-a_2)\rho_2+a_1\tau_1\rho_1+(1-\rho_1-\rho_2)]I_a$ , while death rate due to infection is  $-\alpha_2I_a$ . Accounting for the dynamical flow within the isolated compartment, we observe that the supply source emanating from aware infectives and super spreaders are given by  $a_1\tau_1\rho_1I_a$  and  $a_1\tau_2\gamma_sS_s$ . The proportion that has access to multi-therapies is denoted by  $-(1-a_1)(1-a_2)\delta_h]I_s$  and clearance rate due to both infection death rate and dynamic activity of immune effectors is given by  $-(\alpha_4+v_2\eta_2)I_s$ .

The super spreader are represented by the sixth equation with its source coming from the asymptomatic infectious and aware infectious population depicted by  $\varphi_2e^{-\omega_1\alpha_1}A_u$  and  $(1-\rho_1-\rho_2)I_a$ . The proportion of super spreaders move to isolation compartment is given by  $-a_1\tau_2\gamma_sS_s$ . Here, the amount of virus proliferation in concentrated virions is defined by  $-(1-\rho_1-\rho_2)\varphi_2]e^{-\omega_2\alpha_1}S_s$ , while spatial recovery and death rate arising from infection is described by  $-(\alpha_5+\eta_3)S_s$ . From the seventh equation, we see the influx of hospitalization of the varying infectious

population depicted by  $(1-a_1)(1-a_2)\varphi_1e^{-\omega_1\alpha_1}A_u$  and  $(1-a_1)(1-a_2)[\rho_2I_a+\delta_h]I_s$ . The rate of proliferation of virus under multi-therapies is given by  $-(1-a_1)(1-a_2)[\varphi_1+\rho_2+\delta_h]]e^{-\omega_2\alpha_1}H_i$ . Other clearance rate due to virus infection and recovery rate is given by  $-(\alpha_3+\eta_1)H_i$ . The virulence ingress is represented by the eighth equation with carrying capacity, resource rate and proliferations of super spreaders and hospitalization given by  $s(1-\frac{C_v}{Q})C_v$ ,  $(1-\rho_1-\rho_2)\varphi_2e^{-\omega_2\alpha_1}S_s$  and  $[(1-a_1)(1-a_2)[\varphi_1+\rho_2+\delta_h]]e^{-\omega_2\alpha_1}H_i$ . Only clearance rate is denoted by  $-\mu_vC_v$ .

Equation nine represents the sum population that must have recovered through the period of investigation. Constituting this recovery compartment are from the hospitalized unit  $\eta_1H_i$ , from vaccinated isolated unit  $v_2\eta_2I_s$ , from spatial recovery of super spreaders  $\eta_3S_s$  and from vaccinated susceptible population  $v_1S_p$ . Notably, the recovered populations are expected to be integrated with the susceptible population and observed occasional death rate given by  $-(\mu+\sigma_2)R_p$ . Finally, the activity of the human immune effectors are described by the tenth equation. Here, sustainability of the compartment is constituted by natural source rate  $\zeta_E$  and reversion of the immune system from super spreaders and hospitalized compartment denoted by  $\frac{b_E(S_s+H_i)}{(S_s+H_i)+C_b}E_i$ . Clearance rate due to the concentration of super infectivity and truncated inefficacy from treatment at hospitalization is given by  $-\frac{d_E(S_s+H_i)}{(S_s+H_i)+C_d}E_i$ , while  $-\mu_EE_i$  depicted natural immune effectors death rate.

Of interest is the incorporation of the term  $e^{-\omega_1\alpha_1}$  representing the probability of immature infectious virions produced by the virus ingress that are yet to be virus-producing cells and which constitute the system immune delay lag. On the other hand, the term  $e^{-\omega_2\alpha_1}$  is the probability if immature virions survive through the delay period, where  $\frac{1}{\omega_i}$ ,  $i=1,2$  is the average lifetime for an immature virions. That is,  $(\bullet)e^{-\omega_i\alpha_1}$ ,  $i=1,2$  represent mature viral particles produced at time  $t$ . Thus, a more explicit description of model (1) is depicted by the following schematic flow chart as seen in Fig 1 below.

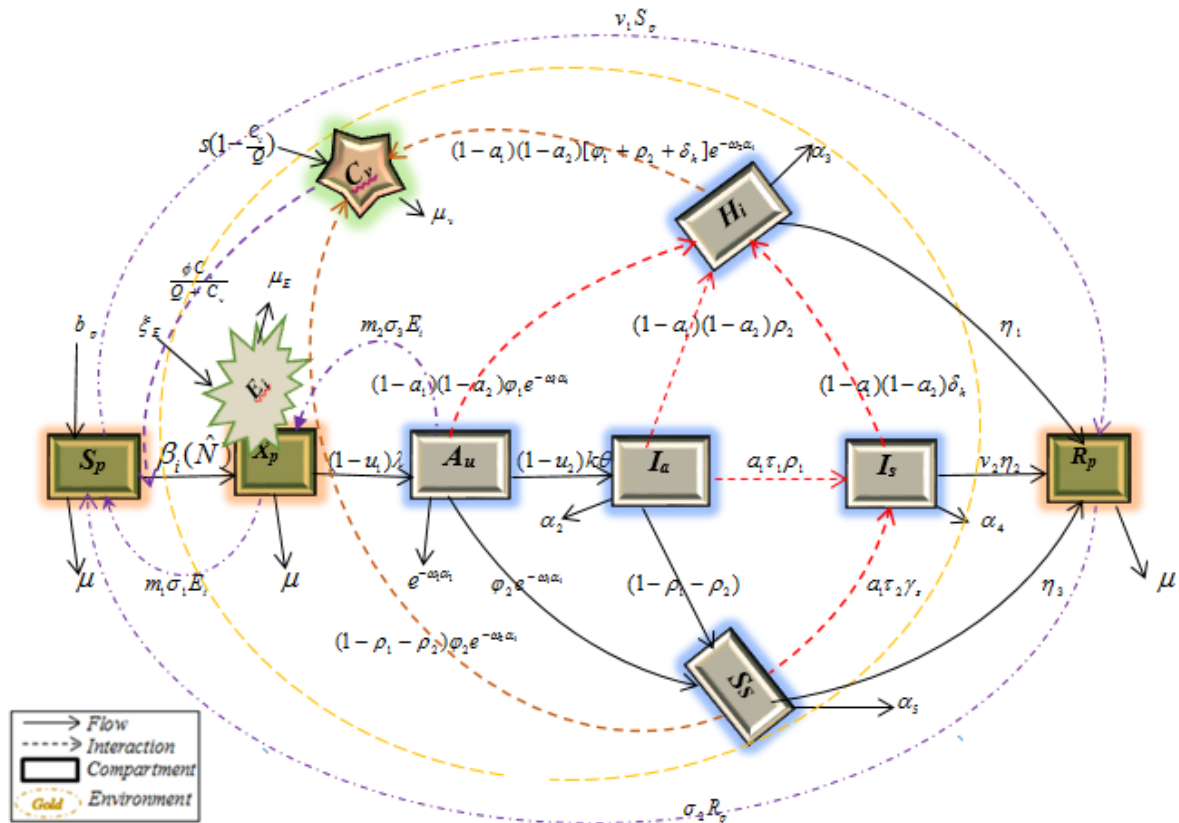


**Fig 1: Schematic representation of COVID-19 infection dynamics under multi-therapy and vaccination control functions**

Aligning with system (1) and Fig 1, it is obvious that the basic model is characterized by a vital index – system mass action (or the incidence rate). This mass action not only determines the biological magnitude of the exponential spread of the virus but acts as a major component of the system reproduction number often denoted by  $\mathfrak{R}_0$ . Notably, the invoking nature of the present model (1) is spanned by the dynamic incorporation and identification of the environmental reservoir of hyper-concentrated viral load  $C_v$  and the biological activities of the immune

effectors  $E_i$ . Moreso, the crystal methodological clinician of triple-bilinear infusion of control functions at designated stages of infection affirmed the novelty of the present investigation. Intuitively, the practical illustration of derived model (1), can be enforced by the description of the state variables and parameters with accompanying initial data emanating University of Calabar Teaching Hospital and from certified data from existing models (see *notes* below Tables 1 and 2). That is, the data for simulation are depicted in Tables 1 and 2 below:

**Table 1: Description of state variables with values – model (1)**

Variables	Dependent variables	Initial values	Units
	Description		
$S_p$	Susceptible population to COVID-19 virus	0.5	$cells/ml^3$
$X_p$	Exposed population	0.3	
$A_u$	Unaware asymptomatic infectious population	0.1	
$I_a$	Aware infective population	0.15	
$I_s$	Isolated infectious population	0.03	
$S_s$	Super-spreaders infectious population	0.05	
$H_i$	Hospitalized infectious population	0.0	
$R_p$	COVID-19 recovered population	0.0	
$C_v$	Aerosol infectious virions	0.025	$copies/ml$
$E_i$	Immune effectors	0.1	

*Note: the initial data for table 1 is generated from UCTH, Calabar and inclusive of modified data from models [2, 22].*

**Table 2: Description of constants and parameter values for model (1)**

Parameter symbols	Parameters and constants Description	Initial values	Units
$b_p$	Source rate of susceptible population	$b_p \leq 10.5$	$ml^3d^{-1}$
$\mu$	Natural death rate for all sub-population	0.1	$day^{-1}$
$k$	Clearance rate of virus	0.25	
$\alpha_{i(i=1,...,5)}$	Death rates due infection at varying stages	0.2;0.3;0.0;0.4;0.5	
$\tau_{i=1,2}$	Rate at which $I_a$ progresses to $I_s$ and $S_s$	0.3, 0.5	
$c_{i(i=1,...,5)}$	Rates of contact of susceptible with various infectious stages	0.5;0.4;0.3;0.2;0.1	
$\eta_{i=1,2,3}$	Rates of recovery from $H_i$ , $I_s$ and $S_s$	0.5; 0.27; 0.13	
$\beta_{i(1,...,5)}$	Probability of interactions of susceptible with varying infectious classes	0.32;0.27;0.175; 0.125;0.05	$ml^3vir^{-1}d^{-1}$
$\phi_{i=1,2}$	Proportions of $A_u$ that progresses to $H_i$ and $S_s$	0.3;0.18	$ml^3d$
$\lambda$	Proportion of $X_p$ becoming $A_u$	0.58	
$\theta$	Proportion of $A_u$ becoming $I_a$	0.32	
$\sigma_{i=1,2,3}$	Proliferation of recovered population to susceptible	0.14; 0.6, 0.24	
$\gamma_s$	Proportion of $S_s$ progressing to $I_s$	0.22	
$\delta_h$	Proportion of $I_s$ progressing to $H_i$	0.14	
$\rho_{i=1,2}$	Proportion of $I_a$ progressing to $I_s$ and $H_i$	0.34; 0.48	
$(1 - \rho_1 - \rho_2)$	Proportion of $I_a$ that progresses to $S_s$	0.18	
$u_{i(i=1,2)}(t)$	Rates at which face-masking and social distancing are used	$u_i \in [0,1]$	
$a_{i(i=1,2)}(t)$	Treatment control functions (HCQ and AZT)	$a_i \in [0,1]$	
$v_{i=1,2}$	Vaccination rates to $S_p$ and $I_s$ compartments	0.06; 0.04	$day^{-1}$
$m_{i=1,2}$	Immune-induced recovery and clearance rates	$1.0 \times 10^{-5}$	$ml^3cell^{-3}d^{-1}$
$\omega_{i=1,2}$	Average lifetime of immature viruses	0.01; 0.01	
$s$	Per-capita rate of aerosol viral load	0.73	$day^{-1}$
$Q$	Carry capacity of aerosol viral load	5.0	$cellsm^{-1}$
$\mu_v$	Virions death rate	0.33	$day^{-1}$
$\phi$	Rate of mass action (incidence rate)	0.5	
$\zeta_E$	Source rate for immune effectors	0.8	$cellsm^{-1}d^{-1}$
$b_E$	Maximum birth rate for immune effectors	0.3	$day^{-1}$
$C_b$	Saturation constant for immune effectors birth	100	$cellsm^{-1}$
$d_E$	Maximum death rate for immune effectors	0.25	$day^{-1}$
$C_d$	Saturation constant for immune effectors death	500	$cellsm^{-1}$
$\mu_E$	Natural death rate for immune effectors	0.1	$day^{-1}$

*Note: the initial data for table 2 is generated from UCTH, Calabar and inclusive of modified data from models [2,22,23,24,25].*

From Tables 1 and 2, it is crystal clear that the choice of our model is motivated by multiple steady states. This quantitative feature explains why some patients develop immune responses sufficient to control infection as depicted by  $m_1E_i\sigma_1$  and  $m_2E_i\sigma_3$  of the exposed unit and the unaware asymptomatic infectious population. These compartments could exhibit somewhat strong COVID-19 specific immune responses capable of containing the infection mostly at the early stage. Whereas, in others, the virus rebounds or fails to contain the virus at all, resulting to decimation of the immune system. Further credence to

the choice of the model is our ability to demonstrate that the mathematical capability of the system state-space is a complete representation of a set of living organisms.

### 3. Mathematical characterization of system state-space

Intuitively, if we assume system (1) to represent a set of living organs, then the state-space compactness requires, then we verify the existence and uniqueness of the system solutions, the positivity of the solution and that the dynamic flow of model (1) is bounded in certain invariant region  $\Omega$ , [37].

**3.1. Existence of solution**

Let

$\Pi : \mathfrak{R} \rightarrow \mathfrak{R}_+^{10}$  such that

$$t \mapsto \begin{pmatrix} S_p(t), & X_p(t), & A_u(t), & I_a(t), & I_s(t), \\ S_s(t), & H_i(t), & R_p(t), & C_v(t), & E_i(t) \end{pmatrix}$$

and

$F : \mathfrak{R} \rightarrow \mathfrak{R}_+^{10}$  such that

$$\Pi(t) \mapsto F(\Pi(t)) = \begin{pmatrix} S_p'(t), & X_p'(t), & A_u'(t), & I_a'(t), & I_s'(t), \\ S_s'(t), & H_i'(t), & R_p'(t), & C_v'(t), & E_i'(t) \end{pmatrix}.$$

Then, system (1) becomes

$$\Pi(t) \mapsto F(\Pi(t)), \quad \Pi(0) = \Pi_0.$$

**Theorem 1** (Existence and Uniqueness)

The system (1) is continuous and satisfies Cauchy-Lipschitz condition.

*Proof*

Here, we invoke the results from the proofs of the existence and uniqueness theorem [23, 37]. Then, we show for one equation and the rest follows the same procedure. Let

$$G(t, s) = \frac{dS_p}{dt} = b_p + m_1 E_i \sigma_1 X_p + \sigma_2 R_p - (1 - u_1 - u_2) \left[ \frac{\phi_{C_v}}{Q + C_v} \left( \sum_{i=1}^5 \beta_i c_i (\hat{N}_i) \right) \right] S_p - (\mu + \nu_1) S_p \dots \dots \dots (3)$$

Then, the partial derives with respect to the susceptible population  $S_p$  gives

$$\frac{\partial G(t, s)}{\partial S} = -(1 - u_1 - u_2) \left[ \frac{\phi_{C_v}}{Q + C_v} \left( \sum_{i=1}^5 \beta_i c_i (\hat{N}_i) \right) \right] - (\mu + \nu_1) \dots \dots \dots (4)$$

We note that the function  $G(t, s)$  and its partial derive  $\frac{\partial G(t, s)}{\partial S}$  are defined and continuous at all point  $(t, s)$ . Similarly, the right-hand functions of other equations and their respective partial derivatives satisfy these conditions. Hence, by the existence and

uniqueness theorem, there exists a unique solution for  $S_p(t), X_p(t), A_u(t), I_a(t), I_s(t), S_s(t), H_i(t), R_p(t), C_v(t)$  and  $E_i(t)$  in some open intervals centered at  $t_0$ . Then, we move to show that the solution satisfies the Lipschitz condition. Now, using Eq. (3), we see that

$$\begin{aligned} |G(t, S_{p(1)}) - G(t, S_{p(2)})| &= \left| \left( b_p + m_1 E_i \sigma_1 X_p + \sigma_2 R_p - (1 - u_1 - u_2) \left[ \frac{\phi_{C_v}}{Q + C_v} \left( \sum_{i=1}^5 \beta_i c_i (\hat{N}_i) \right) \right] S_{p(1)} - (\mu + \nu_1) S_{p(1)} \right) \right. \\ &\quad \left. - \left( b_p + m_1 E_i \sigma_1 X_p + \sigma_2 R_p - (1 - u_1 - u_2) \left[ \frac{\phi_{C_v}}{Q + C_v} \left( \sum_{i=1}^5 \beta_i c_i (\hat{N}_i) \right) \right] S_{p(2)} - (\mu + \nu_1) S_{p(2)} \right) \right| \\ &= \left| (-) \left( (1 - u_1 - u_2) \left[ \frac{\phi_{C_v}}{Q + C_v} \left( \sum_{i=1}^5 \beta_i c_i (\hat{N}_i) \right) \right] + (\mu + \nu_1) \right) (S_{p(1)} - S_{p(2)}) \right| \\ &\leq \left( (1 - u_1 - u_2) \left[ \frac{\phi_{C_v}}{Q + C_v} \left( \sum_{i=1}^5 \beta_i c_i (\hat{N}_i) \right) \right] + (\mu + \nu_1) \right) |S_{p(1)} - S_{p(2)}|. \end{aligned}$$

This implies that

$$|G(t, S_{p(1)}) - G(t, S_{p(2)})| \leq M |S_{p(1)} - S_{p(2)}|,$$

Where,  $M = \left( (1 - u_1 - u_2) \left[ \frac{\phi_{C_v}}{Q + C_v} \left( \sum_{i=1}^5 \beta_i c_i (\hat{N}_i) \right) \right] + (\mu + \nu_1) \right)$  is a Lipschitz constant.

In a similar procedure, we show for the remaining variables satisfying the Lipschitz condition. Thus, there exists a unique solution  $S_p(t), X_p(t), A_u(t), I_a(t), I_s(t), S_s(t), H_i(t), R_p(t), C_v(t), E_i(t)$  for all  $t \geq 0$ .

3.2. Positivity of system solutions

We use the following theorem to show that the system solutions remain positive for all  $t \geq 0$ .

**Theorem 2** (Positivity)

Let system (1) have the initial conditions  $\left\{ \begin{pmatrix} S_p(0), X_p(0), A_u(0), I_a(0), I_s(0) \\ S_s(0), H_i(0), R_p(0), C_v(0), E_i(0) \end{pmatrix} \geq 0 \right\} \in \mathfrak{R}_+^{10}$ . Then, the solution set

$\{S_p(t), X_p(t), A_u(t), I_a(t), I_s(t), S_s(t), H_i(t), R_p(t), C_v(t), E_i(t)\}$  of system (1) is non-negative for all  $t \geq 0$ .

*Proof*

Using exiting results, [37]. Then, from the first equation of system (1), we deduce that for all  $t > 0$ ,

$$\frac{dS_p}{dt} \geq - \left( (1-u_1-u_2) \left[ \frac{\theta C_v}{Q+C_v} \left( \sum_{i=1}^5 \beta_i c_i (\hat{N}_i) \right) \right] + (\mu + v_1) \right) S_p \dots\dots\dots (5)$$

Let  $\tau = \left( (1-u_1-u_2) \left[ \frac{\theta C_v}{Q+C_v} \left( \sum_{i=1}^5 \beta_i c_i (\hat{N}_i) \right) \right] + (\mu + v_1) \right)$ . Then, eq. (5) becomes

$$\frac{dS_p}{dt} = -\tau S_p \dots\dots\dots (6)$$

Integrating, we have

$$\ln |S_p| \geq \int -\tau dt + A \Rightarrow |S_p| \geq e^{\int -\tau dt e^A} \Rightarrow S_p \geq S_{p(0)} e^{\int -\tau dt}$$

Hence,

$$S_p \geq S_{p(0)} e^{\int - \left( (1-u_1-u_2) \left[ \frac{\theta C_v}{Q+C_v} \left( \sum_{i=1}^5 \beta_i c_i (\hat{N}_i) \right) \right] + (\mu + v_1) \right) dt} \geq 0 \dots\dots\dots (7)$$

Where  $S_{p(0)}$  is the susceptible population at  $t = 0$ .

Similarly, we obtain for the rest of the equations of system (1). Therefore, any solution of system (1) is such that the set  $\left\{ \begin{pmatrix} S_p(0), X_p(0), A_u(0), I_a(0), I_s(0), S_s(0), H_i(0), R_p(0), C_v(0), E_i(0) \end{pmatrix} \geq 0 \right\} \in \mathfrak{R}_+^{10}$  and the proof is completed.

Next, in the following theorem, we show that it is sufficient to consider the dynamic flow of system (1) in a certain region – the invariant region,  $\Omega$ .

**Theorem 3** (Boundedness)

All solution of model (1) is bounded and positively invariant in the region

$$\Omega_D = \Omega_N \times \Omega_v \dots\dots\dots (8)$$

where

$$\Omega_N = \left\{ (S_p, X_p, A_u, I_a, I_s, S_s, H_i, R_p, E_i) \in \mathfrak{R}_+^9 : 0 \leq (S_p(t) + X_p(t) + \dots + E_i(t)) \leq \frac{b_p}{\mu} \right\} \dots\dots\dots (9)$$

and

$$\Omega_v = \left\{ C_v \in \mathfrak{R}_+ : 0 \leq C_v(t) \leq \frac{\varepsilon b_p}{\mu_v \mu} \right\} \dots\dots\dots (10)$$

for all  $\varepsilon = s \left( 1 - \frac{C_v}{Q} \right) C_v + (1 - \rho_1 - \rho_2) \varphi_2 e^{-\omega_2 \alpha_1} S_s + [(1 - a_1)(1 - a_2)[\varphi_1 + \rho_2 + \delta_h]] e^{-\omega_2 \alpha_1} H_i$ .

*Proof*

Invoking existing results for boundedness of solutions [2, 23, 26, 37], then, we begin by splitting the model (1) into human and virus populations  $N(t), C_v(t)$ . Then, taking the human population from model (1), we have

$$\frac{dN}{dt} = b_p - \mu N - \hat{\alpha} \hat{N} + \zeta_E - \mu_v E_i$$

If population is free of virus, then  $\hat{\alpha} = 0$ . That is, we have

$$\frac{dN}{dt} = b_p - \mu N + \zeta_E - \mu_v E_i$$

or

$$\frac{dN}{dt} + \mu N \leq b_p + \zeta_E - \mu_v E_i.$$

Integrating in the presence of initial conditions, we obtain

$$N(t) \leq \frac{(b_p + \zeta_E)}{\mu} + \left( N(0) - \frac{(b_p + \zeta_E)}{\mu} \right) e^{-\mu t}.$$

Thus, taking the limit, we have

$$\lim_{t \rightarrow \infty} N(t) \leq \frac{(b_p + \zeta_E)}{\mu} \dots \dots \dots (11)$$

Similarly,

$$\frac{dC_v}{dt} = \varepsilon(S_s + H_i) - \mu_v C_v \leq \varepsilon \frac{b_p}{\mu} - \mu_v C_v,$$

or

$$\lim_{t \rightarrow \infty} N(t) \leq \frac{\varepsilon b_p}{\mu_v \mu} \dots \dots \dots (12)$$

From Eqs (11) and (12), we see that the human and virus populations are biologically feasible in the regions (9) and (10), which is defined by Eq. (8) i.e.

$$\Omega_D = \Omega_N \times \Omega_v \subset \mathfrak{R}_+^9 \times \mathfrak{R}_+.$$

Therefore, the solution of model (1) with initial conditions, is bounded in the invariant region (8) for all  $t \in [0, \infty)$ . hence, the system is well posed.

Next, in our coming section, we shall derive the system threshold number and identify the biological equilibria for model (1).

**4. Stability analysis for derived COVID-19 model**

Clearly, the analytical prediction for the steady state of system (1) and their local stability derivation is challenging due to the form and number of nonlinearities. None-the less, our interest is to investigate the model multiple locally asymptomatic stability as well as the global conditions.

**4.1 Existence of steady states for COVID-19 model**

Let the vectorial capacity of the model state-space be denoted by  $p$ , such that

$$p = (S_p, X_p, A_u, I_a, I_s, S_s, H_i, R_p, E_i, C_v).$$

Then, system (1) may be represented by

$$\frac{dp(t)}{dt} = f(t, p; z) \dots \dots \dots (13)$$

where  $f(t, p; z)$  is the right-side of the ODEs of system (1) and  $z$  is the vector parameters as specified in Table 2; and the following is computed.

**4.1. 1. COVID-19 free-equilibrium (C-19FE) states**

At C-19FE, it is assumed that there exists no infection in the population and so no virus in the environment. This implies that

$$S_p = X_p = A_u = I_a = I_s = S_s = H_i = R_p = E_i = C_v = 0.$$

Thus, the C-19FE for model (1) is given by

$$E^0 = (S_p^0, X_p^0, A_u^0, I_a^0, I_s^0, S_s^0, H_i^0, R_p^0, E_i^0, C_v^0)$$

or

$$E^0 = (S_p, 0, 0, 0, 0, 0, 0, 0, 0, 0) \dots \dots \dots (14)$$

with  $S_p = \frac{b_p}{\mu}$ . Eq. (14) depicts a COVID-19 model under zero disease steady state.

**4.1.2. COVID-19 endemic equilibrium (C-19EE) states**

Let any arbitrary endemic equilibrium of system (1) be represented by

$$E^* = (S_p^*, X_p^*, A_u^*, I_a^*, I_s^*, S_s^*, H_i^*, C_v^*, R_p^*, E_i^*) \dots \dots \dots (15)$$

Such that

$$N^* = S_p^* + X_p^* + A_u^* + I_a^* + I_s^* + S_s^* + H_i^* + R_p^* + E_i^*.$$

Then, by solving system (1) using Eq. (13) and equating the right side of each of the equations to zeros, i.e., for the first equation, we have

$$0 = b_p - \beta_i(\hat{N})S_p - (\mu + v_1)S_p$$

or

$$S_p^* = \frac{b_p}{\beta_i^* + (\mu + v_1)}.$$

Taking on the second equation, we have

$$0 = \beta_i^*(\hat{N})S_p^* + m_2 E_i^* \sigma_3 A_u^* - (1 - u_1)\lambda X_p^* - q_1 X_p^*$$

or

$$0 = \beta_i^*(\hat{N})S_p^* - (\lambda + q_1)X_p^*$$

This implies that

$$X_p^* = \frac{\beta_i^*(\hat{N})S_p^*}{(\lambda + q_1)} = \left( \frac{b_p}{\lambda + q_1} \right) \frac{\beta_i^*}{(\beta_i^* + \mu + v_1)},$$

Where  $q_1 = \mu + m_1 \sigma_1$ .

Thus, solving for the rest of the state variables gives the required results for  $E^*$  as:

$$\left\{ \begin{aligned} S_p^* &= \frac{b_p}{\beta_i^* + (\mu + v_1)} \\ X_p^* &= \left( \frac{b_p}{\lambda + q_1} \right) \frac{\beta_i^*}{(\beta_i^* + \mu + v_1)} \\ A_u^* &= \left( \frac{\lambda b_p}{(\Pi_1 + q_2)(\lambda + q_1)} \right) \frac{\beta_i^*}{(\beta_i^* + \mu + v_1)} \\ I_a^* &= \left( \frac{k\theta e^{-\omega_1 \alpha_1} \lambda b_p}{\Pi_2(\Pi_1 + q_2)(\lambda + q_1)} \right) \frac{\beta_i^*}{(\beta_i^* + \mu + v_1)} \\ I_s^* &= 0 \\ S_s^* &= \left( \frac{(\varphi_2 + (1 - \rho_1 - \rho_2)k\theta)e^{-\omega_1 \alpha_1} \lambda b_p}{\Pi_3[(\Pi_1 + q_2)(\lambda + q_1)][\Pi_2(\Pi_1 + q_2)(\lambda + q_1)]} \right) \left( \frac{\beta_i^*}{(\beta_i^* + \mu + v_1)} \right)^2 \\ H_i^* &= \left( \frac{(\varphi_1 + \rho_2)k\theta e^{-\omega_1 \alpha_1} \lambda b_p}{\Pi_4[(\Pi_1 + q_2)(\lambda + q_1)][\Pi_2(\Pi_1 + q_2)(\lambda + q_1)]} \right) \left( \frac{\beta_i^*}{(\beta_i^* + \mu + v_1)} \right)^2 \\ C_v^* &= \frac{\sqrt{(1 - \rho_1 - \rho_2)\varphi_2 e^{-\omega_1 \alpha_1} S_s^* + (\varphi_1 + \rho_2 + \delta_h)e^{-\omega_1 \alpha_1} H_i^*}}{sQC_v^{-1} - s - \mu_v QC_v^{-1}} \\ R_p^* &= \frac{\eta_1(\varphi_1 + \rho_2)k\theta e^{-\omega_1 \alpha_1} \lambda b_p + \eta_3[\varphi_2 + (1 - \rho_1 - \rho_2)k\theta e^{-\omega_1 \alpha_1} \lambda b_p + v_1 b_p]}{q_6\{\Pi_4[(\Pi_1 + q_2)(\lambda + q_1)][\Pi_2(\Pi_1 + q_2)(\lambda + q_1)][\Pi_3[(\Pi_1 + q_2)(\lambda + q_1)][\Pi_2(\Pi_1 + q_2)(\lambda + q_1)]]\}} \left( \frac{\beta_i^*}{(\beta_i^* + \mu + v_1)} \right)^5 \quad (16) \\ E_i^* &= \frac{\xi_E[(S_s^* + H_i^*)(C_b + C_d)]}{b_E(S_s^* + H_i^*) - d_E(S_s^* + H_i^*) - \mu_E} \end{aligned} \right.$$

Where  $\left\{ \begin{aligned} \Pi_1 &= (k\theta + \varphi_1 + \varphi_2)e^{-\omega_1 \alpha_1}, & \Pi_2 &= \rho_2 + (1 - \rho_1 - \rho_2) + \alpha_2, \\ \Pi_3 &= [(1 - \rho_1 - \rho_2)\varphi_2]e^{-\omega_2 \alpha_1} + q_4, & \Pi_4 &= (\varphi_1 + \varphi_2 + \delta_h)e^{-\omega_2 \alpha_1} + q_5 \\ \hat{\Pi}_5 &= (1 - \rho_1 - \rho_2)\varphi_2 e^{-\omega_2 \alpha_1}, & \hat{\Pi}_6 &= (\varphi_1 + \varphi_2 + \delta_h)e^{-\omega_2 \alpha_1}, & \hat{s} &= s \left( 1 - \frac{C_v}{Q} \right) \end{aligned} \right. \dots\dots\dots (17)$

With

$$\left\{ \begin{aligned} q_1 &= \mu + m_1 E_i \sigma_1, & q_2 &= \mu + m_2 E_i \sigma_3, \\ q_3 &= \alpha_4 + v_2 \eta_2, & q_4 &= \alpha_5 + \eta_3, & \dots\dots\dots (18) \\ q_5 &= \alpha_3 + \eta_1, & q_6 &= \mu + \sigma_2 \end{aligned} \right.$$

Now, substituting Eq. (16) into Eq. (13) at  $\beta_i^* = 0$  define the point at which C-19FE exists and which satisfies Eq. (14). Therefore, for  $\beta_i^* \neq 0$ , the endemic state for system (1) denoted by  $E^*$  is completely defined by Eq. (16) and which agree with Eq. (15).

**4.2. System reproduction number  $\mathfrak{R}_0$ , for a hypo-hyper infectious COVID-19 model**

Biologically, the intuitive understanding of the dynamics of infectious diseases lies in the ability to

define and compute the disease transmission rate, known as the system basic reproduction number denoted by  $\mathfrak{R}_0$ . From [27] view point, reproduction number  $\mathfrak{R}_0$  represents the number of secondary infections produced in a completely susceptible population by a typically infectious individual in its infective duration. Then, advancing the course of deriving and computing  $\mathfrak{R}_0$ , we invoke the formidable next generation matrix method by [28] to derive as follows our COVID-19 reproduction number.

Let

$$f = \begin{pmatrix} (1-u_1-u_2) \left[ \frac{\phi C_v}{Q+C_v} \left( \sum_{i=1}^5 \beta_i c_i (\hat{N}_i) \right) \right] S_p \\ 0 \\ 0 \\ 0 \\ 0 \\ 0 \\ 0 \end{pmatrix}, V = \begin{pmatrix} (\lambda + q_1) X_p - m_2 E_i \sigma_3 A_u \\ (\Pi_1 + q_2) A_u - \lambda X_p \\ \Pi_2 I_a - k \theta e^{-\omega_1 \alpha_1} A_u \\ (\delta_h + q_3) I_s - (a_1 \tau_1 \rho_1 I_a + a_2 \tau_2 \gamma_s S_s) \\ (a_2 \tau_2 \gamma_s + \Pi_3) S_s - (\varphi_2 e^{-\omega_1 \alpha_1} A_u + (1 - \rho_1 - \rho_2) I_a) \\ \Pi_4 H_i - (\varphi_1 e^{-\omega_1 \alpha_1} A_u + (\rho_2 I_a + \delta_h I_s)) \\ \mu_v C_v - (\hat{s} C_v + \hat{\Pi}_1 S_s + \hat{\Pi}_2 H_i) \end{pmatrix},$$

Where  $f$  is the rate of appearance of new infection and  $V = V^- - V^+$  such that  $V^-$  and  $V^+$  are the rates of transfer of the infected individuals into the class by any

other means and out of the compartments. That is, using Eqs (17) and (18), the transfer rates of infected in and out of compartments are given by

$$V^- = \begin{pmatrix} (\lambda + q_1) X_p \\ (\Pi_1 + q_2) A_u \\ \Pi_2 I_a \\ (\delta_h + q_3) I_s \\ (a_2 \tau_2 \gamma_s + \Pi_3) S_s \\ \Pi_4 H_i \\ \mu_v C_v \end{pmatrix} \text{ and } V^+ = \begin{pmatrix} m_2 E_i \sigma_3 A_u \\ \lambda X_p \\ k \theta e^{-\omega_1 \alpha_1} A_u \\ (a_1 \tau_1 \rho_1 I_a + a_2 \tau_2 \gamma_s S_s) \\ (\varphi_2 e^{-\omega_1 \alpha_1} A_u + (1 - \rho_1 - \rho_2) I_a) \\ (\varphi_1 e^{-\omega_1 \alpha_1} A_u + (\rho_2 I_a + \delta_h I_s)) \\ (\hat{s} C_v + \hat{\Pi}_1 S_s + \hat{\Pi}_2 H_i) \end{pmatrix}.$$

Computing the derivatives of  $f$  and  $v$  with respect to  $x = (X_p, A_u, I_a, I_s, S_s, H_i, C_v)$  at C-19FE  $E^0$  and using Eq. (14), we obtain the linearized form for  $F$  as:

$$F = \frac{\partial f(E^0)}{\partial x_j} = \begin{pmatrix} \psi \tilde{\lambda} (\beta_1 c_1 \frac{b_p}{\mu}) & \psi \tilde{\lambda} (\beta_2 c_2 \frac{b_p}{\mu}) & \psi \tilde{\lambda} (\beta_3 c_3 \frac{b_p}{\mu}) & \psi \tilde{\lambda} (\beta_4 c_4 \frac{b_p}{\mu}) & \psi \tilde{\lambda} (\beta_5 c_5 \frac{b_p}{\mu}) & 0 & 0 \\ 0 & 0 & 0 & 0 & 0 & 0 & 0 \\ 0 & 0 & 0 & 0 & 0 & 0 & 0 \\ 0 & 0 & 0 & 0 & 0 & 0 & 0 \\ 0 & 0 & 0 & 0 & 0 & 0 & 0 \\ 0 & 0 & 0 & 0 & 0 & 0 & 0 \end{pmatrix},$$

Where  $\psi = (1 - u_1 - u_2)$  and  $\tilde{\lambda} = \frac{\phi C_v}{Q + C_v}$ .

Similarly, the linearization for  $V$  is given by

$$V = \frac{\partial V(E^0)}{\partial x_j} = \begin{pmatrix} (\lambda + q_1) & -m_2 E_i \sigma_3 & 0 & 0 & 0 & 0 & 0 \\ -\lambda & (\Pi_1 + q_2) & 0 & 0 & 0 & 0 & 0 \\ 0 & -k \theta e^{-\omega_1 \alpha_1} & \Pi_2 & 0 & 0 & 0 & 0 \\ 0 & 0 & -a_1 \tau_1 \rho_1 & (\delta_h + q_3) & -a_2 \tau_2 \gamma_s & 0 & 0 \\ 0 & -\varphi_2 e^{-\omega_1 \alpha_1} & -(1 - \rho_1 - \rho_2) & 0 & \Lambda_1 & 0 & 0 \\ 0 & -\varphi_1 e^{-\omega_1 \alpha_1} & -\rho_2 & -\delta_h & 0 & \Pi_4 & 0 \\ 0 & 0 & 0 & 0 & -\hat{\Pi}_1 & -\hat{\Pi}_1 & (\mu_v - \hat{s}) \end{pmatrix},$$

Where  $\Lambda_1 = (a_2 \tau_2 \gamma_s + \Pi_3)$ . Thus, using the computed approach by [2, 23], the spectral radius of the present

system reproduction number denoted by  $\mathfrak{R}_0 = \rho(FV^{-1})$  is computed as:

$\mathfrak{R}_0 = \rho(FV^{-1}) = \frac{\psi \tilde{\lambda} b_p}{\mu_v \mu} \left( \frac{\beta_1 c_1}{(\lambda + q_1)} + \frac{\beta_2 c_2}{(\Pi_1 + q_2)} + \frac{\beta_3 c_3}{\Pi_2} + \frac{\beta_4 c_4}{\Lambda_1} + \frac{\beta_5 c_5}{\Pi_4} \right)$  Eq. (21) represent the rate of dynamic infection under systemic control functions with computed value  $\mathfrak{R}_{0(2)} \cong -3.01 < 1$ . Here, we note that

or

$$\mathfrak{R}_0 = \psi \tilde{\lambda} \left( \sum_{j=1}^5 R_j \right) \dots\dots\dots (19)$$

where  $j = 1, \dots, 5$  represent the contributive reproduction number of each of the system infectious state variables with  $\psi = (1 - u_1 - u_2)$  and  $\tilde{\lambda} = \frac{\phi C_v}{Q + C_v}$ .

For a completely untreated COVID-19 scenario, the reproduction number is in Eq. (19) with control function  $(u_i, a_i, v_i, m_i) = 0, i = 1, 2$  is transformed to the form:

$$\mathfrak{R}_{0(1)} = \frac{\tilde{\lambda} b_p}{\mu_v \mu} \left( \frac{\beta_1 c_1}{(\lambda + \mu)} + \frac{\beta_2 c_2}{(\Pi_1 + \mu)} + \frac{\beta_3 c_3}{\Pi_2} + \frac{\beta_4 c_4}{\Pi_3} + \frac{\beta_5 c_5}{\Pi_4} \right) \dots\dots\dots (20)$$

Eq. (20) represent the exponential rate of highly infectious aerosol viral load under zero control function with computed value  $\mathfrak{R}_{0(1)} \cong 10.159 > 1$  in reality, under cogent dynamic control function, the system reproduction number is bound to varies. That is, for control functions  $(u_i, a_i, v_i, m_i) > 0, i = 1, 2$ , Eq. (19) is expanded to become

$$\mathfrak{R}_{0(2)} = \rho(FV^{-1}) = \frac{\psi \tilde{\lambda} b_p}{\mu_v \mu} \left( \frac{\beta_1 c_1}{(\lambda + q_1)} + \frac{\beta_2 c_2}{(\Pi_1 + q_2)} + \frac{\beta_3 c_3}{\Pi_2} + \frac{\beta_4 c_4}{\Lambda_1} + \frac{\beta_5 c_5}{\Pi_4} \right) \dots\dots\dots (21)$$

unlike the study by [2], where the scope of the study was limited to human-to-human transmission mode, the present study, which is characterized by environment-to-human (hypo-infectious) and human-to-human (hyper-infectious) is clearly depicted by the environmental index  $\frac{\tilde{\lambda}}{\mu_v}$  among other parameters of Eq.

(19). Next, we discuss the system local stability analysis in terms of system reproduction number  $\mathfrak{R}_0$ .

**4.3 Local stability analysis in terms of  $\mathfrak{R}_0$**

We determine the local stability analysis of system (1) by invoking the eigenvalues of the linearized Jacobian matrix as done in [29]. The following theorem satisfies the local stability of COVID-19 under hypo-hyper infectious scenario with determined  $\mathfrak{R}_0$ .

**Theorem 4**

The existence of C-19FE ( $E^0$ ) for model (1) is completely characterized by locally asymptotic stability if  $\mathfrak{R}_0 < 1$  and locally asymptotically unstable if  $\mathfrak{R}_0 > 1$ .

**Proof**

Invoking the existence results from [2, 22, 23], then letting  $J$  represent the Jacobian matrix of system (1), we have the C-19FE ( $E^0$ ) derived as:

$$J_{(E^0)} = \begin{pmatrix} -\chi_1 & -D_1 & -D_2 & -D_3 & 0 & -D_4 & -D_5 & 0 & \sigma_2 & 0 \\ 0 & -\chi_2 & D_2 & D_3 & 0 & D_4 & D_5 & 0 & 0 & 0 \\ 0 & -\lambda & -\chi_3 & 0 & 0 & 0 & 0 & 0 & 0 & 0 \\ 0 & 0 & k\theta e^{-\alpha_1 \alpha_1} & -\Pi_2 & 0 & 0 & 0 & 0 & 0 & 0 \\ 0 & 0 & 0 & 0 & -(\delta_h + \alpha_4) & 0 & 0 & 0 & 0 & 0 \\ 0 & 0 & \varphi_2 e^{-\alpha_1 \alpha_1} & (1 - \rho_1 - \rho_2) & 0 & -\chi_4 & 0 & 0 & 0 & 0 \\ 0 & 0 & \varphi_1 e^{-\alpha_1 \alpha_1} & \rho_2 & \delta_h & 0 & -\chi_5 & 0 & 0 & 0 \\ 0 & 0 & 0 & 0 & 0 & \hat{\Pi}_1 & \hat{\Pi}_2 & -(\mu_v - \hat{s}) & 0 & 0 \\ v_1 & 0 & 0 & 0 & 0 & \eta_3 & \eta_1 & 0 & -q_6 & 0 \\ 0 & 0 & 0 & 0 & 0 & A_{10,6} & A_{10,7} & 0 & 0 & -A_{10,10} \end{pmatrix} \dots\dots\dots (22)$$

where  $D_i = \psi \tilde{\lambda} \frac{b_p}{\mu} \beta_i c_i, i = 1, \dots, 5, \chi_1 = (\mu + v_1), \chi_2 = (D_1 + \lambda + \mu), \chi_3 = (\Pi_1 + \mu), \chi_4 = [(1 - \rho_1 - \rho_2)\varphi_2 e^{-\alpha_2 \alpha_1} + q_4], \hat{\Pi}_1 = (1 - \rho_1 - \rho_2)\varphi_2 e^{-\alpha_2 \alpha_1}, \hat{\Pi}_2 = (\varphi_1 + \rho_2 + \delta_h) e^{-\alpha_2 \alpha_1}, \chi_5 = [(\varphi_1 + \rho_2 + \delta_h) e^{-\alpha_2 \alpha_1} + q_5], A_{10,6} = A_{10,7} = \frac{b_E C_b E_i}{(S_s + H_i + C_b)^2} - \frac{d_E C_d E_i}{(S_s + H_i + C_d)^2}$  and  $A_{10,10} = \left[ \left( \frac{b_E}{S_s + H_i + C_b} + \frac{d_E}{S_s + H_i + C_d} \right) (S_s + H_i) + \mu_E \right]$ .

Now, taking the eigenvalues of  $J_{(E^0)}$ , we see that all the diagonal entries are all negative i.e.,  $-\chi_1, -\chi_2, -\chi_3, -\Pi_2, -(\delta_h + \alpha_4), -\chi_4, -\chi_5, -(\mu_v - \hat{s}), -q_6$  and  $-A_{10,10}$ . Therefore, the infection is locally asymptotically stable for all  $\mathfrak{R}_0 < 1$ , which satisfies Eq. (19), implying that  $\mathfrak{R}_0 = \sum_{i=1}^5 (\psi \lambda R_j) < 1, j=1, \dots, 5$ .

This completes the proof.

Next, we consider cases where infections persist in the population. In this case, an endemic equilibrium is bound to exist. Then, we must verify the existence of the system endemic equilibrium point for our model (1).

**4.4. COVID-19 endemic equilibrium (C-19EE) in terms of  $\mathfrak{R}_0$**

The following theorem completely satisfies the existence of an endemic equilibrium for system (1).

**Theorem 5**

The existence of an endemic equilibrium in an infectious COVID-19 of the model (1) is feasible provided only  $\mathfrak{R}_0 > 1$ .

**Proof**

Let  $E^* = (S_p^*, X_p^*, A_u^*, I_a^*, I_s^*, S_s^*, H_i^*, C_v^*, R_p^*, E_i^*)$  define the C-19EE of system (1). Suppose we equate each of the equations of system (1) to zero and then use the results of Eq. (16), we see that the differential sum of system (1) at C-19EE as derived in the models [30, 31] is given by

$$b_p - \mu N - \hat{\alpha} \hat{N} + \zeta_E - \mu_E E_i = 0$$

or

$$\mu N^* = b_p - \hat{\alpha} \hat{N}^* + \zeta_E - \mu_E E_i$$

Differentiating with respect to  $N^*$  for all  $\hat{\alpha} = 0$ , we obtain

$$N^* = \frac{(b_p + \zeta_E)}{\mu} \dots \dots \dots (22)$$

which corresponds to the fact that at C-19FE,  $\beta_i^* = 0$ . At endemic equilibrium, incidence rate  $\beta_i^* > 0$ , which implies system (1) exhibits endemic properties. Relating Eq. (22) with Eq. (19), we have

$$\beta_i^* (1 + \beta_i^* \hat{Q} - \mathfrak{R}_0) = 0,$$

from which we obtain

$$\beta_i^* = \frac{\mathfrak{R}_0 - 1}{\hat{Q}} \dots \dots \dots (23)$$

for all  $\mathfrak{R}_0 > 0$  and having  $\hat{Q}$  as disease constant derived from Eqs (17) and (18). This completes the proof.

**4.5. Global stability analysis for COVID-19 model**

The authors [2] have answered some basic questions of stability of C-19FE and C-19EE both at local and global cases for what is considered a motivating model for the present study. Notably, the global stability of the endemic equilibrium for the present model is, however, much more difficult to analyze. None-the-less, we will approach this demanding task using the method of Lyapunov functions in conjunction with Volterra-Lyapunov stable matrices to systematically address this uphill challenge, noting the following notations.

**Notations and preliminaries 1**

The following fundamental results (notations, definitions, lemmas, and theorems) are used to determine all square matrices of Volterra-Lyapunov stable matrices [32].

*Notation 1.* We write a matrix  $M > 0 (< 0)$ , if  $M$  is symmetric positive (negative) definite.

*Definition 1.* A nonsingular  $n \times n$  matrix  $M$  is diagonally stable (or positive stable) if there exists a positive diagonal  $n \times n$  matrix  $Q$  such that  $QM + M^T Q^T < 0$ .

*Definition 2.* A nonsingular  $n \times n$  matrix  $M$  is diagonally stable (or positive stable) if there exists a positive diagonal  $n \times n$  matrix  $Q$  such that  $QM + M^T Q^T > 0$ .

From Definitions 1 and 2, it become obvious that a matrix  $M$  is Volterra-Lyapunov stable if and only if its negative matrix  $-M$ , is diagonally stable.

*Lemma 1.* Let  $M$  be an  $n \times n$  real matrix. Then, all the eigenvalues of  $M$  have negative (positive) real parts if and only if there exists a matrix  $K > 0$  such that  $KM + M^T K^T < 0 (> 0)$ .

*Lemma 2.* Let  $P = \begin{bmatrix} p_{11} & p_{12} \\ p_{21} & p_{22} \end{bmatrix}$  be a  $2 \times 2$  matrix.

Then,  $P$  is Volterra-Lyapunov stable if and only if  $p_{11} < 0, p_{22} < 0$  and  $\det(P) = p_{11}p_{22} - p_{12}p_{21} > 0$ .

*Notation 2.* Given any  $n \times n$  matrix  $M$ , let  $\tilde{M}$  denote the  $(n-1) \times (n-1)$  matrix derived from  $M$  by deleting its last row and last column.

*Lemma 3.* Let  $P = [p_{ij}]$  be a nonsingular  $n \times n$  matrix ( $n \geq 2$ ) and  $Q = \text{diag}(q_1, \dots, q_n)$  be a positive diagonal  $n \times n$  matrix. Let  $B = P^{-1}$  matrix. Suppose if  $p_{mm} > 0, \tilde{Q}\tilde{B} + (\tilde{M}\tilde{B})^T > 0, \tilde{Q}\tilde{B} + (\tilde{M}\tilde{B})^T > 0$  and  $\tilde{Q}\tilde{P} + (\tilde{Q}\tilde{P})^T > 0$ . Then, it is possible to choose  $p_n > 0$  such that  $QP + (\tilde{Q}\tilde{P})^T > 0$ .

**Lemma 4.** Consider a COVID-19 model of the form

$$\begin{cases} \frac{dX_1}{dt} = F(X_1, X_2) \\ \frac{dX_2}{dt} = G(X_1, X_2) \end{cases} \dots\dots\dots (24)$$

$$X_1 = \begin{bmatrix} S_p \\ I_s \\ R_p \\ E_i \end{bmatrix}, \quad X_2 = \begin{bmatrix} X_p \\ A_u \\ I_a \\ S_s \\ H_i \\ C_v \end{bmatrix}.$$

with  $G(X_1, X_2) = 0$ , where  $X_1 \in \mathfrak{R}^m$  denotes the uninfected population and  $X_2 \in \mathfrak{R}^n$  denotes the infection population;  $X_0 = (X_1^E, 0)$  denotes the C-19FE of the system. Furthermore, assume that the following condition holds:

(C<sub>1</sub>) For  $\frac{dX_1}{dt} = F(X_1, 0)$ ,  $X_1^E$  is globally asymptotically stable.

(C<sub>2</sub>)  $G(X_1, X_2) = MX_2 - \hat{G}(X_1, X_2)$ , with  $\hat{G}(X_1, X_2) \geq 0$  for all  $(X_1, X_2) \in \Phi$ , where the Jacobian matrix

$$M = \frac{\partial G}{\partial x_2}(X_1^E, 0),$$

has all nonnegative off-diagonal elements and  $X$  is the region where the model makes biological meaning. Then, the C-19EE,  $X_0 = (X_1^E, 0)$  is globally asymptotically stable provided that  $\mathfrak{R}_0 < 1$ .

**4.5.1. Global stability of C-19FE (untreated)**

Here, the system global stability for C-19FE is discussed using the existing results from theorem [33].

**Theorem 6**

Let the fixed point  $E^0 = (\frac{b_p}{\mu}, 0, 0, 0, 0, 0, 0, 0, \frac{\xi_E}{\mu_E})$

is globally asymptotically stable equilibrium for the system (1) for all  $\mathfrak{R}_0 < 1$ . Then, the conditions in Eq. (24) of lemma 4 are satisfied.

**Proof**

Using the result of model [2] and invoking Lemma 2 for system (1), then we have

If  $X_p = A_u = I_a = S_s = H_i = C_v = 0$ , then the uninfected sub-systems (i.e.,  $S_p, I_s, R_p, E_i$ ) becomes

$$\begin{cases} \frac{dS_p}{dt} = b_p - \mu S_p \\ \frac{dI_s}{dt} = 0 \\ \frac{dR_p}{dt} = 0 \\ \frac{dE_i}{dt} = \xi_E - \mu_E E_i \end{cases}$$

or

$$X_1 = \begin{cases} \frac{dS_p}{dt} = b_p - \mu S_p \\ \frac{dE_i}{dt} = \xi_E - \mu_E E_i \end{cases},$$

which has the following solutions

$$S_p(t) \leq \frac{b_p}{\mu} + \left( S_p(0) - \frac{b_p}{\mu} \right) e^{-\mu t} \dots\dots\dots (25)$$

and

$$E_i(t) \leq \frac{\xi_E}{\mu_E} + \left( E_i(0) - \frac{\xi_E}{\mu_E} \right) e^{-\mu_E t} \dots\dots\dots (26)$$

Clearly, from Eq. (25),  $S_p(t) \rightarrow \frac{b_p}{\mu}$  as  $t \rightarrow \infty$  irrespective of the value of  $S_p(0)$ . Moreover, the same can be said of Eq. (26). Therefore, we have shown that condition (C<sub>1</sub>) of lemma 2 holds for system (1). Next, we consider the right-hand side of the infectious system for  $X_2$  i.e.,

$$\frac{dX_2}{dt} = G(X_1, X_2) = \begin{pmatrix} \hat{q}_1 X_p + \psi \lambda \sum_{i=1}^5 \beta_i c_i \\ \lambda X_p - (\Pi_1 + q_2) A_u \\ k \theta e^{-\alpha_1 \alpha_i} A_u - (\Pi_2 + \alpha_2) I_a \\ \varphi_2 e^{-\alpha_1 \alpha_i} A_u + (1 - \rho_1 - \rho_2) I_a - \Pi_3 S_s \\ \varphi_1 e^{-\alpha_1 \alpha_i} A_u + \rho_2 I_a - \Pi_4 H_i \\ \hat{s} C_v + \hat{\Pi}_1 S_s + \hat{\Pi}_2 H_i - \mu_v C_v \end{pmatrix}.$$

Applying condition (C<sub>2</sub>) of lemma 2, then we have

$$\frac{dX_2}{dt} = G(X_1, X_2) = \begin{pmatrix} -\hat{q}_1 + m_1 & m_2 & m_3 & m_4 & m_5 & 0 \\ \lambda & -(\Pi_1 + q_2) & 0 & 0 & 0 & 0 \\ 0 & k\theta e^{-\omega_1 \alpha_1} & -(\Pi_2 + \alpha_2) & 0 & 0 & 0 \\ 0 & \varphi_2 e^{-\omega_1 \alpha_1} & (1 - \rho_1 - \rho_2) & -\Pi_3 & 0 & 0 \\ 0 & \varphi_1 e^{-\omega_1 \alpha_1} & \rho_2 & 0 & -\Pi_4 & 0 \\ 0 & 0 & 0 & \hat{\Pi}_1 & \hat{\Pi}_2 & -(\mu_v - \hat{s}) \end{pmatrix} \begin{pmatrix} X_p \\ A_u \\ I_a \\ S_s \\ H_i \\ C_v \end{pmatrix} - \begin{pmatrix} \beta_i \frac{b_p}{\mu} - \beta_i S_p \\ 0 \\ 0 \\ 0 \\ 0 \\ 0 \end{pmatrix} \dots\dots\dots (27)$$

Where

$$\hat{q}_1 = (\lambda + q_1), m_1 = \psi \lambda \beta_1 c_1 \frac{b_p}{\mu N}, m_2 = \psi \lambda \beta_2 c_2 \frac{b_p}{\mu N},$$

$$m_3 = \psi \lambda \beta_3 c_3 \frac{b_p}{\mu N}, m_4 = \psi \lambda \beta_4 c_4 \frac{b_p}{\mu N} \text{ and}$$

$$m_5 = \psi \lambda \beta_5 c_5 \frac{b_p}{\mu N}, \text{ noting that other parameters have}$$

been earlier defined in Eq. (17). By condition (C<sub>2</sub>) of lemma 2, we see that Eq. (27) becomes

$$\frac{dX_2}{dt} = MX_2 - \hat{G}(X_1, X_2),$$

Which implies that *M* equal to the first term of the right-hand side of Eq. (27) and  $\hat{G}(X_1, X_2)$  is equal to the last term. Then, it is obvious that  $S_p \leq \frac{b_p}{\mu}$ , which implies that  $G(X, Y) \geq 0$  for all  $(X, Y) \in \mathfrak{R}_+^6$ . Notably, the matrix *M* is an *Q*-matrix since all its off-diagonal elements are nonnegative. Hence, this proves that global stability for C-19FE (*E*<sup>0</sup>).

**4.5.2. Global stability of C-19EE model for  $\hat{\alpha}_i = 0$**

Our aim here is to show that the endemic equilibrium of COVID-19 model for  $\hat{\alpha}_i = 0$  is globally asymptotically stable. We achieve this goal by adopting the classical method of Lyapunov functions in combination with the Volterra-Lyapunov matrix as has been explored [30]. The following definitions and theorems provide the enabling environment for our investigation.

$$R_D = \left\{ (S_p, X_p, A_u, I_a, I_s, S_s, H_i, C_v, R_p, E_i) \in \mathfrak{R}_+^{10} : N \leq \frac{b_p + \xi_E}{\mu} : S_p + X_p + \dots + E_i(t) \leq \frac{b_p + \xi_E}{\mu} \right\},$$

which is positively invariant set in  $\mathfrak{R}^{10}$ . Visibly, is the fact that  $N = N^* = \frac{b_p + \xi_E}{\mu}$  as  $t \rightarrow \infty$ . We then prove the system global stability by constructing the following Lyapunov function. Suppose

$$V = \sum_{i=1}^{10} z_i (N_i - N_i^*)^2 \dots\dots\dots (28)$$

**Definition 3 (Lyapunov function)**

Let the function *V*(*x*) be a region of state-space  $\mathfrak{R}_D$  and containing an equilibrium point *X*<sup>\*</sup>. Then, this point *X*<sup>\*</sup> is called a Lyapunov function if the following conditions are satisfied [26, 34]:

- i. *V*(*x*) is continuous and has continuous first-order partial derivatives.
- ii. *V*(*x*) has a unique minimum point at *X*<sup>\*</sup> with respect to all other points in the region  $\mathfrak{R}_D$ .
- iii. The function  $V'(x(t)) = \bar{V}V(x)f(x)$  satisfies  $V'(x(t)) \leq 0$  for all  $x(t) \in \mathfrak{R}_D$ .

**Theorem 7**

If there exists a Lyapunov function for an equilibrium point *X*<sup>\*</sup>, then *X*<sup>\*</sup> is a stable equilibrium point. Moreso, if the function  $V'(x(t)) \leq 0$  for all  $x(t) \in \mathfrak{R}_D$  for all  $x(t) \in \mathfrak{R}_D$ , then the stability is asymptotic.

**Theorem 8**

Let *V* be the Lyapunov function defined for system (1). Then, the global stability of the system endemic equilibrium for COVID-19 (C-19EE) exists provided the time derivative  $\frac{dL}{dt} \leq 0$ .

**Proof**

We invoke results from existing Lyapunov proves [2, 30, 35]. Then, let the biological feasible domain for system (1) be given by

Where  $z_i > 0$  is positive Lyapunov constants, *N<sub>i</sub>* is the population of *i*<sup>th</sup> compartment, *N<sub>i</sub>*<sup>\*</sup> is the equilibrium value of *N<sub>i</sub>* and *V*, a continuous and differentiable Lyapunov function. Then, computing the time derivative of *V*, along the trajectories of system (1), we have

$$\square V = 2z_i \sum_{i=1}^{10} (N_i - N_i^*) \frac{dN_i}{dt}, \quad i = 1, \dots, 10 \dots\dots\dots (29)$$

That is, using system (1) in Eq. (29) and accounting for Eq. (18), we have

$$\begin{aligned} \square \hat{V} = & 2z_1(S_p - S_p^*) \left[ \begin{aligned} & m_1\sigma_1(E_i X_p - E_i^* X_p^*) + \sigma_2(R_p - R_p^*) - \frac{(1-u_1-u_2)}{N^*} \hat{\lambda} \left( \begin{aligned} & \beta_1 c_1 (X_p S_p - X_p^* S_p^*) + \beta_2 c_2 (A_u S_p - A_p^* S_p^*) \\ & + \beta_3 c_3 (I_a S_p - I_a^* S_p^*) + \beta_4 c_4 (S_s S_p - S_s^* S_p^*) \\ & + \beta_5 c_5 (H_i S_p - H_i^* S_p^*) \end{aligned} \right) \\ & -(\mu + v_i)(S_p - S_p^*) \end{aligned} \right] \\ & + 2z_2(X_p - X_p^*) \left[ \begin{aligned} & \frac{(1-u_1-u_2)}{N^*} \hat{\lambda} \left( \begin{aligned} & \beta_1 c_1 (X_p S_p - X_p^* S_p^*) + \beta_2 c_2 (A_u S_p - A_p^* S_p^*) \\ & + \beta_3 c_3 (I_a S_p - I_a^* S_p^*) + \beta_4 c_4 (S_s S_p - S_s^* S_p^*) \\ & + \beta_5 c_5 (H_i S_p - H_i^* S_p^*) \end{aligned} \right) \\ & + m_2 \sigma_3 (E_i A_u - E_i^* A_u^*) - (1-u_1)\lambda(X_p - X_p^*) - q_1(X_p - X_p^*) \end{aligned} \right] \\ & + 2z_3(A_u - A_u^*) \left[ (1-u_1)\lambda(X_p - X_p^*) - \Pi_1(A_u - A_u^*) - q_2(A_u - A_u^*) - m_2 \varphi_1(A_u - A_u^*) \right] \\ & + 2z_4(I_a - I_a^*) \left[ (1-u_2)k\theta e^{-\alpha_1 \alpha_1} (A_u - A_u^*) - [\Pi_2 + \alpha_2](I_a - I_a^*) \right] \\ & + 2z_5(I_s - I_s^*) \left[ a_1 \tau_1 \rho_1 (I_a - I_a^*) + a_1 \tau_2 \gamma_s (S_s - S_s^*) - (1-a_1)(1-a_2)\delta_h(I_s - I_s^*) - q_3(I_s - I_s^*) \right] \\ & + 2z_6(S_s - S_s^*) \left[ (1-\rho_1 - \rho_1)(I_a - I_a^*) + \varphi_2(A_u - A_u^*) - a_1 \tau_2 \gamma_s (S_s - S_s^*) - \Pi_3(S_s - S_s^*) \right] \\ & + 2z_7(H_i - H_i^*) \left[ \begin{aligned} & (1-a_1)(1-a_2)\varphi_1 e^{-\alpha_1 \alpha_1} (A_u - A_u^*) + (1-a_1)(1-a_2)[\rho_2(I_a - I_a^*) \\ & + \delta_h(I_s - I_s^*)] - \Pi_4(H_i - H_i^*) \end{aligned} \right] \\ & + 2z_8(C_v - C_v^*) \left[ \hat{s}(C_v - C_v^*) + \hat{\Pi}_1(S_s - S_s^*) + \hat{\Pi}_1(H_i - H_i^*) - \mu_v(C_v - C_v^*) \right] \\ & + 2z_9(R_p - R_p^*) \left[ \eta_1(H_i - H_i^*) + v_2 \eta_2(I_s - I_s^*) + \eta_3(S_s - S_s^*) - q_6(R_p - R_p^*) \right] \\ & + 2z_{10}(E_i - E_i^*) \left[ \hat{b}_E(E_i - E_i^*) - \hat{d}_E(E_i - E_i^*) - \mu_v(E_i - E_i^*) \right] \dots \dots \dots (30) \end{aligned}$$

where  $\hat{b}_E = \frac{b_E[(S_s - S_s^*) + (H_i - H_i^*)]}{[(S_s - S_s^*) + (H_i - H_i^*)] + C_b}$  and  $\hat{d}_E = \frac{d_E[(S_s - S_s^*) + (H_i - H_i^*)]}{[(S_s - S_s^*) + (H_i - H_i^*)] + C_d}$ .

Then, by adding the expression  $\beta_i c_i \hat{N} S_p^*$  for all  $\hat{N} = (X_p, A_u, I_a, S_s, H_i)$  into the first and second square brackets, the following results are obtain:

$$\begin{aligned} \square \hat{V} = & 2z_1(S_p - S_p^*) \left[ \begin{aligned} & m_1\sigma_1(E_i X_p - E_i^* X_p^*) + \sigma_2(R_p - R_p^*) - \frac{(1-u_1-u_2)}{N^*} \hat{\lambda} \left( \begin{aligned} & -\beta_1 c_1 (X_p S_p - X_p^* S_p^*) + \beta_1 c_1 X_p S_p^* - \beta_1 c_1 X_p^* S_p^* \\ & -\beta_2 c_2 (A_u S_p - A_p^* S_p^*) + \beta_2 c_2 A_u S_p^* - \beta_2 c_2 A_u^* S_p^* \\ & -\beta_3 c_3 (I_a S_p - I_a^* S_p^*) + \beta_3 c_3 I_a S_p^* - \beta_3 c_3 I_a^* S_p^* \\ & -\beta_4 c_4 (S_s S_p - S_s^* S_p^*) + \beta_4 c_4 S_s S_p^* - \beta_4 c_4 S_s^* S_p^* \\ & -\beta_5 c_5 (H_i S_p - H_i^* S_p^*) + \beta_5 c_5 H_i S_p^* - \beta_5 c_5 H_i^* S_p^* \end{aligned} \right) \\ & -(\mu + v_i)(S_p - S_p^*) \end{aligned} \right] \\ & + 2z_2(X_p - X_p^*) \left[ \begin{aligned} & \frac{(1-u_1-u_2)}{N^*} \hat{\lambda} \left( \begin{aligned} & -\beta_1 c_1 (X_p S_p - X_p^* S_p^*) + \beta_1 c_1 X_p S_p^* - \beta_1 c_1 X_p^* S_p^* \\ & -\beta_2 c_2 (A_u S_p - A_p^* S_p^*) + \beta_2 c_2 A_u S_p^* - \beta_2 c_2 A_u^* S_p^* \\ & -\beta_3 c_3 (I_a S_p - I_a^* S_p^*) + \beta_3 c_3 I_a S_p^* - \beta_3 c_3 I_a^* S_p^* \\ & -\beta_4 c_4 (S_s S_p - S_s^* S_p^*) + \beta_4 c_4 S_s S_p^* - \beta_4 c_4 S_s^* S_p^* \\ & -\beta_5 c_5 (H_i S_p - H_i^* S_p^*) + \beta_5 c_5 H_i S_p^* - \beta_5 c_5 H_i^* S_p^* \end{aligned} \right) \\ & + m_2 \sigma_3 (E_i A_u - E_i^* A_u^*) - (1-u_1)\lambda(X_p - X_p^*) - q_1(X_p - X_p^*) \end{aligned} \right] \\ & + 2z_3(A_u - A_u^*) \left[ (1-u_1)\lambda(X_p - X_p^*) - \Pi_1(A_u - A_u^*) - q_2(A_u - A_u^*) - m_2 \varphi_1(A_u - A_u^*) \right] \end{aligned}$$

$$\begin{aligned}
 &+2z_4(I_a - I_a^*) \left[ (1-u_2)k\theta e^{-\omega_1\alpha_1} (A_u - A_u^*) - [\Pi_2 + \alpha_2](I_a - I_a^*) \right] \\
 &+2z_5(I_s - I_s^*) \left[ a_1\tau_1\rho_1(I_a - I_a^*) + a_1\tau_2\gamma_s(S_s - S_s^*) - (1-a_1)(1-a_2)\delta_h(I_s - I_s^*) - q_3(I_s - I_s^*) \right] \\
 &+2z_6(S_s - S_s^*) \left[ (1-\rho_1 - \rho_1)(I_a - I_a^*) + \varphi_2(A_u - A_u^*) - a_1\tau_2\gamma_s(S_s - S_s^*) - \Pi_3(S_s - S_s^*) \right] \\
 &+2z_7(H_i - H_i^*) \left[ \begin{aligned} &(1-a_1)(1-a_2)\varphi_1 e^{-\omega_1\alpha_1} (A_u - A_u^*) + (1-a_1)(1-a_2)[\rho_2(I_a - I_a^*)] \\ &+ \delta_h(I_s - I_s^*) - \Pi_4(H_i - H_i^*) \end{aligned} \right] \\
 &+2z_8(C_v - C_v^*) \left[ \hat{s}(C_v - C_v^*) + \hat{\Pi}_1(S_s - S_s^*) + \hat{\Pi}_1(H_i - H_i^*) - \mu_v(C_v - C_v^*) \right] \\
 &+2z_9(R_p - R_p^*) \left[ \eta_1(H_i - H_i^*) + v_2\eta_2(I_s - I_s^*) + \eta_3(S_s - S_s^*) - q_6(R_p - R_p^*) \right] \\
 &+2z_{10}(E_i - E_i^*) \left[ \hat{b}_E(E_i - E_i^*) - \hat{d}_E(E_i - E_i^*) - \mu_v(E_i - E_i^*) \right] \dots\dots\dots (31)
 \end{aligned}$$

The compact form of Eq. (31) is written as:

$$\mathbb{V} = L(TX + X^T T^T)L^T \dots\dots\dots (32)$$

Where  $L = (S_p - S_p^*, X_p - X_p^*, A_u - A_u^*, \dots\dots\dots, E_i - E_i^*)$ ,  $X = \text{diag}(z_1, z_2, \dots\dots\dots, z_{10})$  and

$$T = \begin{pmatrix} \phi_1 & -\phi_3 & -\phi_5 & -\phi_8 & 0 & -\phi_{12} & -\phi_{15} & 0 & 0 & 0 \\ \phi_2 & \phi_4 & \phi_6 & \phi_9 & 0 & \phi_{13} & -\phi_{16} & 0 & 0 & 0 \\ 0 & 0 & -\phi_7 & 0 & 0 & 0 & 0 & 0 & 0 & 0 \\ 0 & 0 & 0 & -\phi_{10} & 0 & 0 & 0 & 0 & 0 & 0 \\ 0 & 0 & 0 & 0 & -\phi_{11} & 0 & 0 & 0 & 0 & 0 \\ 0 & 0 & 0 & 0 & 0 & -\phi_{14} & 0 & 0 & 0 & 0 \\ 0 & 0 & 0 & 0 & 0 & 0 & -\phi_{17} & 0 & 0 & 0 \\ 0 & 0 & 0 & 0 & 0 & 0 & 0 & \phi_{18} & 0 & 0 \\ 0 & 0 & 0 & 0 & 0 & 0 & 0 & 0 & -\phi_{19} & 0 \\ 0 & 0 & 0 & 0 & 0 & 0 & 0 & 0 & 0 & \phi_{20} \end{pmatrix}, \dots\dots\dots (33)$$

With

$$\begin{aligned}
 \phi_1 &= \frac{(1-u_1-u_2)}{N^*} \hat{\lambda} (-\beta_1 c_1 X_p - \beta_2 c_2 A_u - \beta_3 c_3 I_a - \beta_4 c_4 S_s - \beta_5 c_5 H_i) - (\mu + v_i) + m_1 \sigma_1 + \sigma_2, \\
 \phi_2 &= \frac{(1-u_1-u_2)}{N^*} \hat{\lambda} (\beta_1 c_1 X_p + \beta_2 c_2 A_u + \beta_3 c_3 I_a + \beta_4 c_4 S_s + \beta_5 c_5 H_i), \quad \phi_3 = \frac{(1-u_1-u_2)}{N^*} \hat{\lambda} \beta_1 c_1 S_p^* \\
 \phi_4 &= \frac{(1-u_1-u_2)}{N^*} \hat{\lambda} \beta_1 c_1 S_p^* - ((1-u_1)\lambda + q_1) + m_2 \sigma_3 E_i, \quad \phi_{5,6} = \frac{(1-u_1-u_2)}{N^*} \hat{\lambda} \beta_2 c_2 S_p^*, \\
 \phi_7 &= (\Pi_1 - q_2) + (1-u_1), \quad \phi_{8,9} = \frac{(1-u_1-u_2)}{N^*} \hat{\lambda} \beta_3 c_3 S_p^*, \quad \phi_{10} = (\Pi_2 - \alpha_2) + (1-u_1)k\theta e^{-\omega_1\alpha_1}, \\
 \phi_{11} &= [(1-q_1)(1-q_2)\delta_h + q_3] - a_1\tau_1\rho_1 - a_2\tau_2\gamma_s, \quad \phi_{12,13} = \frac{(1-u_1-u_2)}{N^*} \hat{\lambda} \beta_4 c_4 S_p^*, \\
 \phi_{14} &= [a_2\tau_2\gamma_s - \varphi_2 e^{-\omega_1\alpha_1} - (1-\rho_1 - \rho_2)], \quad \phi_{15,16} = \frac{(1-u_1-u_2)}{N^*} \hat{\lambda} \beta_5 c_5 S_p^*, \\
 \phi_{17} &= (\Pi_4 - (1-a_1)(1-a_2)\alpha_1 e^{-\omega_1\alpha_1} - (1-a_1)(1-a_2)\rho_2 - \delta_h), \quad \phi_{18} = (\hat{s} - \mu_v) + \hat{\Pi}_1 + \hat{\Pi}_2, \\
 \phi_{19} &= (q_6 - \eta_1 - v_2\eta_2 - \eta_3) \text{ and } \phi_{20} = (\hat{b}_E - \hat{d}_E - \mu_E).
 \end{aligned}$$

We now proceed to verify the global asymptotic stability of  $L$  by showing that  $X$  defined in Eq. (32) is Volterra-Lyapunov stable or  $-X$  is diagonal stable. The following lemmas are necessary and the proofs of which can be sorted, [30].

**Lemma 5.** For the matrix  $X$  defined in Eq. (32), let  $D = -\tilde{X}$ , then  $D$  is diagonal stable.

**Remark 1.** Lemma 3 guarantee that  $D = -\tilde{X}$  is diagonal stable.

**Lemma 6.** For the matrix  $X$  defined in Eq. (32), the matrix  $B = -\tilde{X}^{-1}$ , then  $D$  is diagonal stable.

**Remark 2.** Lemma 3 is used again to show that guarantee that  $-\tilde{B}^{-1}$  is Volterra-Lyapunov stable.

**Theorem 9**

The matrix  $X$  defined in Eq. (32), is Volterra-Lyapunov stable.

**Proof**

Based on lemma 3 and lemma 5 and since  $-X_{10,10} > 0$  i.e.  $\phi_{20}$ , there exists a positive diagonal matrix  $T$  such that  $T(-X) + (-X)^T T^T > 0$ . Thus,  $TX + X^T T^T < 0$ .

**Theorem 10**

The endemic equilibrium,  $E^* = (S_p^*, X_p^*, \dots, E_i^*)$  of model (1) is globally asymptotically stable.

**Proof**

Based on Lemma 3, Lemma 5 and lemma 9, we obtain  $\frac{dV}{dt} < 0$  when  $E \neq E^*$  and  $E$  are not the  $S$ -axis (a set of measure zero). Therefore, by Volterra-Lyapunov stable, it implies that the endemic equilibrium of system (1) is globally asymptotically stable.

**5. Numerical computations**

Having gone through the analytical predictions of our derived basic model (1), it becomes obvious that we can then validate these predictions numerically, noting that analytical illustrations are imperative due to the complex nonlinearity of our model. Notably, the strength of our numerical simulation is emphatically a function of the system reproduction numbers for both

off/on control functions ( $\mathfrak{R}_{0(1)}$  and  $\mathfrak{R}_{0(2)}$ ). That is, the overall effect of  $\mathfrak{R}_0 = (\mathfrak{R}_{0(1)} + \mathfrak{R}_{0(2)})$  to the system state-space will be computed. The essence is to afford us a clear view of the impact of the induced control functions.

Furthermore, we shall simulate the system stability and endemic equilibrium, following the introduction of a vaccine (*BNT162b2* or any other recommended vaccines) alongside dual bilinear control functions (two nonpharmaceutical: face-masking and social distancing; and two pharmaceuticals: hydroxylchloroquine – HCQ and azithromycin – AZT). Remarkably, the testing of the entire model shall explore for its simulations, in-built rkfixed Runge-Kutta of the order of precision 4 on a Mathcad surface in relation to Tables 1 and 2.

**5.1. Numerical computation for  $\mathfrak{R}_{0(1)}, \mathfrak{R}_{0(2)}$**

In subsection 4.2, we present the derivation of the system reproduction numbers for both off and on-set treatment scenarios with corresponding analytic values at  $\mathfrak{R}_{0(1)} = 10.159$  and  $\mathfrak{R}_{0(2)} = -3.01$  respectively. These values are biologically the initial values at the onset of infection and prior to the application of control functions. Thus, Fig. 2(a-b), below depicts the graphic images for the impact of these reproduction numbers for model (1).

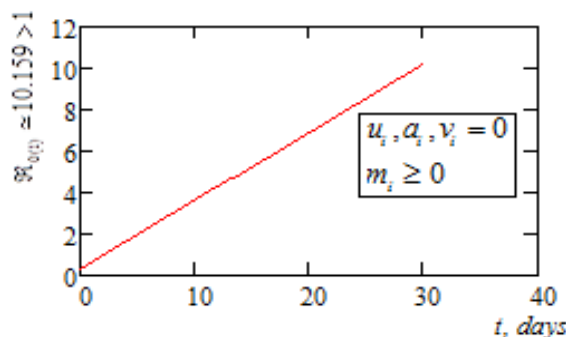


Fig 2(a): System reproduction number for COVID -19 under off-treatment with  $\beta_i(\hat{N}) = 1.69 \times 10^{-4}$

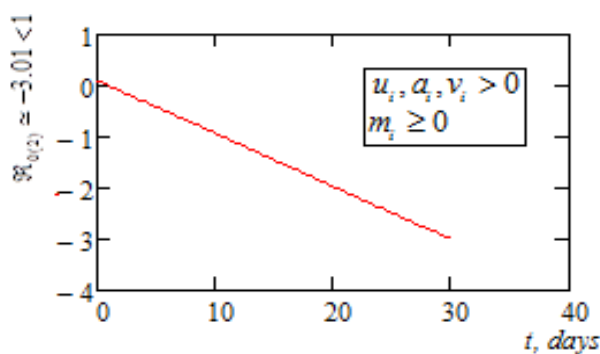


Fig 2(b): System reproduction number for COVID -19 under onset-treatment with  $\beta_i(\hat{N}) = -3.379 \times 10^{-5}$

**Fig 2(a-b): Graphical images of system reproduction numbers for off/onset – treatment of COVID-19,  $\mathfrak{R}_{0(1)}, \mathfrak{R}_{0(2)}$**

Fig 2(a), depicts a rapid inclined smooth curve indicating the dynamic spread of COVID-19 virus under off-treatment scenario. A value range of  $0.5 \leq R_{0(1)} \leq 10.159$  is observed, which portraint population extinction if no intervention for all  $t_f \leq 30$  days. Fig 2(b), portraint the drastic and rapid decline in the spread of the virus, following the methodological introduction of varying control functions. Rate of transmission is seen reduced to  $0.5 \leq R_{0(2)} \leq -3.01$ , which could lead to terminal spread of the virus for all  $t_f \leq 30$  days.

**5.2. Numerical computation of derived basic system (I), with  $u_i, a_i, v_i = 0$  and  $m_i \geq 0 \forall i = 1, 2$**

Following the dynamic contribution of the system force of infection  $\beta_i(\hat{N})$ , which is embedded in the system reproduction number  $\mathfrak{R}_0 = (\mathfrak{R}_{0(1)} + \mathfrak{R}_{0(2)})$ ,

we compute as in Appendix A1 and A2, the overall impact of these parameters on COVID-19 transmission within the state space as seen in Fig. 3(a-j), below, noting that  $u_i, a_i, v_i = 0$  with immune effectors  $m_i \geq 0 \forall i = 1, 2$ .

From Fig. 3(a), asymptotic infection is observed within the first twelve days of virus contact with the susceptible population. Hence, a steady growth of the population is seen at the early stage until after the 12th day, where infection started manifesting resulting in a rapid decline. This implies consumption of the susceptible, which is only sustained via the natural recruitment rate. That is asymptomatic stage  $\approx 0.5 \leq S_p(t) \leq 67.132$  for all  $t_f \leq 12$  days. Thereafter, symptomatic stage  $\approx 0.5 \leq S_p(t) \leq 10$  for all  $12 \leq t_f \leq 30$  days.

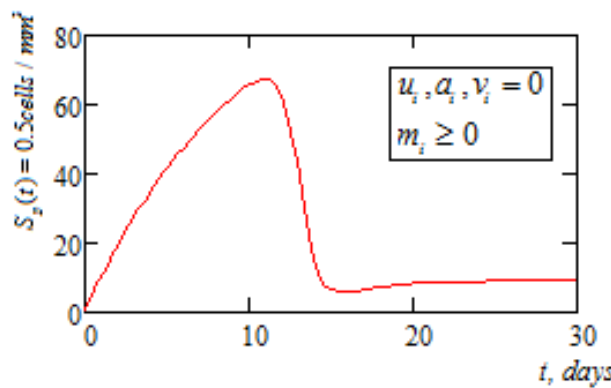


Fig 3(a): Susceptible popn under COVID -19 dynamics with off-treatment and  $\mathfrak{R}_{0(1)} = 10.159 > 1$

Fig. 3(b), depicts the exposed population with asymptomatic infection within the first  $t_f \leq 10$  days. Thereafter, the spread of infection is seen escalating through  $10 \leq t_f \leq 12$  days, with  $0.035 \leq X_p(t) \leq 36.71$

$cells/ml^3$  and then decline to symptomatic stability with values at  $36.71 \leq X_p(t) \leq 18 cells/ml^3$  for all  $12 \leq t_f \leq 30$  days.

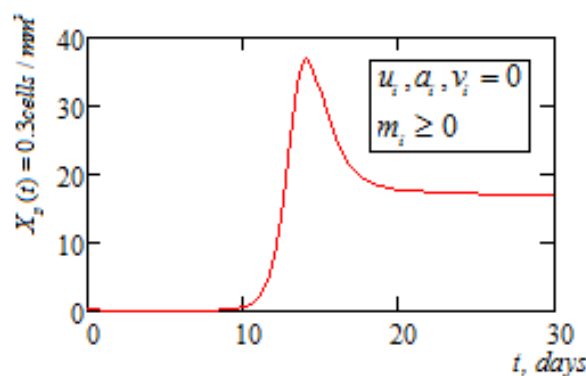


Fig 3(b): Exposed popn under COVID -19 dynamics with off-treatment and  $\mathfrak{R}_{0(1)} = 10.159 > 1$

From Fig. 3(c), the unaware infective exhibits initial asymptomatic stability at the first 12 days and thereafter exhibits accelerated inclination with value  $0.041 \leq A_u(t) \leq 24.596 cells/ml^3$  for all  $12 \leq t_f \leq 16$

days. Unaware infections declined to symptomatic stability with value  $24.596 \leq A_u(t) \leq 15 cells/ml^3$  for all  $12 \leq t_f \leq 30$  days.

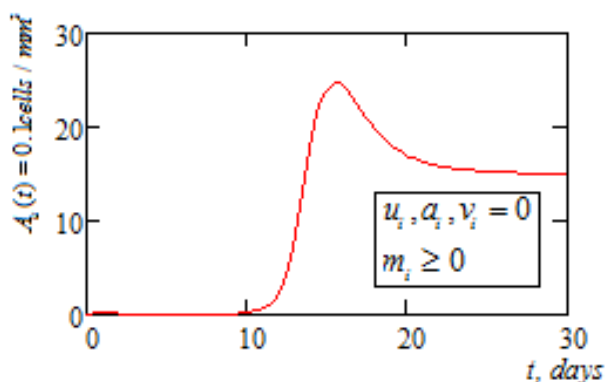


Fig 3(c): Unaware infectives under COVID -19 dynamics with off-treatment and  $\mathfrak{R}_{0(c)} = 10.159 > 1$

In Fig. 3(d), the pattern of spread is seen sustained to reduced rate of infection under aware infectives. Observed is a concave asymptomatic early stage due to awareness for all  $t_f \leq 12$  days. The trend of

the unaware infective is observed but with reduced rate of infection i.e.  $3.806 \times 10^{-3} \leq I_a(t) \leq 1.882 \text{ cells} / \text{ml}^3$  for all  $16 \leq t_f \leq 30$  days.

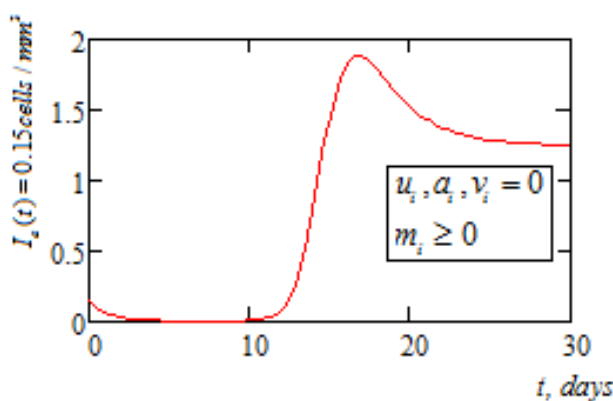


Fig 3(d): Aware infectives under COVID -19 dynamics with off-treatment and  $\mathfrak{R}_{0(d)} = 10.159 > 1$

The isolated population in Fig. 3(e), is seen to decline to near population extinction in the first ten days of isolation without any control measures i.e.  $0.03 \leq I_i(t) \leq 2.764 \times 10^{-9}$  for all  $t_f \leq 10$  days and attain symptomatic stability thereafter for all  $10 \leq t_f \leq 30$

days. This implies that an isolated population without control measures leads to population termination with insignificant surviving population coming from natural recruitment rate  $b_p = 0.5 \text{ cells} / \text{ml}^3$ .

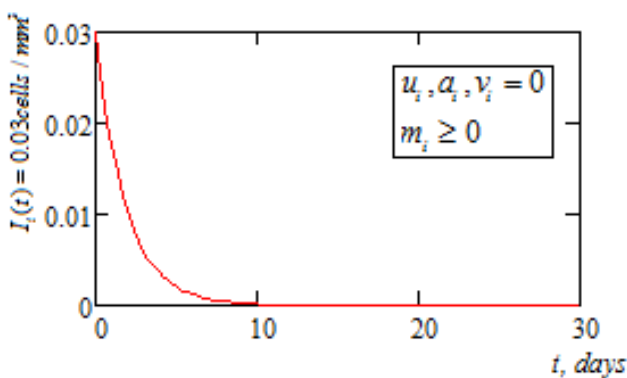


Fig 3(e): Isolated infectives under COVID -19 dynamics on off-treatment and  $\mathfrak{R}_{0(e)} = 10.159 > 1$

From Fig. 3(f), the super-spreader exhibited initial asymptomatic stability at the early period of

infection with value of  $0 \leq S_s(t) \leq 0.015 \text{ cells} / \text{ml}^3$  for all  $t_f \leq 12$  days. Symptomatic manifestation of the virus

at  $0.015 \leq S_s(t) \leq 6.208 \text{ cells/ml}^3$  and then declining with undulating curve terminating at  $S_s(t) \leq 4.218$

$\text{cells/ml}^3$  for all  $12 \leq t_f \leq 30$  days.

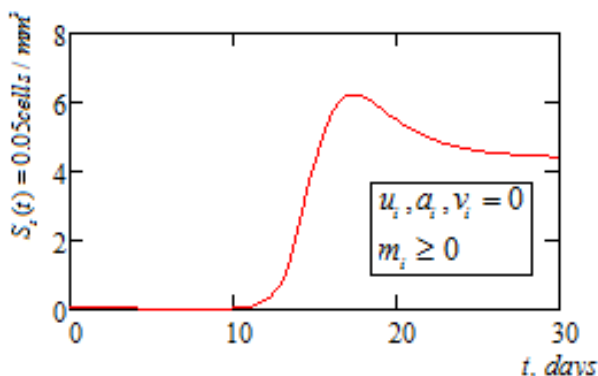


Fig 3(f): Super-spreaders under COVID -19 dynamics with off-treatment and  $\mathfrak{R}_{(0)} > 1$

Hospitalized population as depicted in Fig. 3(g), exhibited similar behavior to that of super-spreader compartment, which also indicates the lack of any control measures, i.e., asymptomatic stability with  $0.0 \leq H_i(t) \leq 0.0 \text{ cells/ml}^3$  for all  $t_f \leq 12$  days.

Symptomatic manifestation of the virus at  $0.0 \leq H_i(t) \leq 5.193 \text{ cells/ml}^3$  and then declining with undulating curve terminating at  $H_i(t) \leq 3.712 \text{ cells/ml}^3$  for all  $12 \leq t_f \leq 30$  days.

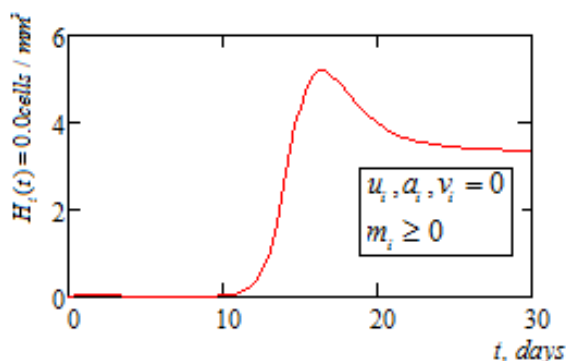


Fig 3(g): Hospitalized infectives under COVID -19 dynamics with off-treatment and  $\mathfrak{R}_{(0)} = 10.159 > 1$

Fig. 3(h), representing the vector reservoir exhibits an initial smooth inclination indicating the mass force of infection within the first-eighteen days with value of  $0.025 \leq C_v(t) \leq 7.275$  for all  $0 \leq t_f \leq 18$

days. Thereafter, decline to slight stability with value at  $C_v(t) \leq 6.152$  for all  $18 \leq t_f \leq 30$  days. This implies that under off-treatment, the reservoir of aerosol viral load could overwhelm the entire environment.

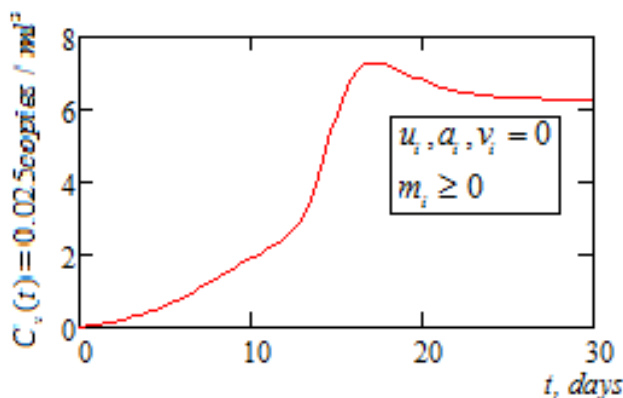


Fig 3(h): Aerosol infectious virions dynamics on off-treatment and  $\beta_i(\hat{N}) = 1.69 \times 10^{-4}$

Recovered compartment as in Fig. 3(i), shows insignificant recovery at the early stage of the spread of the virus with asymptomatic value of  $R_p(t) \leq 0.0125$  cells/ml<sup>3</sup> for all  $t_f \leq 10$  days. Recovery proportions inclined thereafter, which could be attributed to the

increase in adaptive immune response and the awareness of the presence of the virus coupled with the application of nonpharmaceutical. Slight decline at the tail of the investigation with value at  $R_p(t) \leq 3.2$  cells/ml<sup>3</sup> for all  $18 \leq t_f \leq 30$  days.

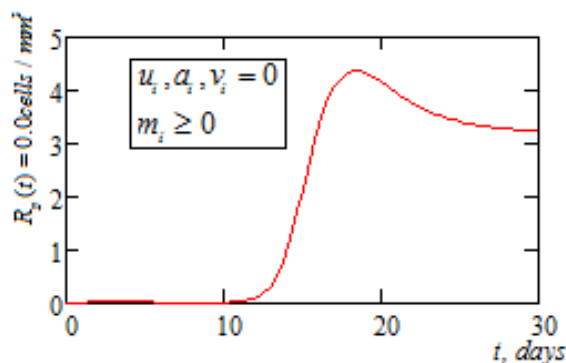


Fig 3(i): Recover infectives under COVID -19 dynamics with off-treatment and  $\mathfrak{R}_{(0)} = 10.159 > 1$

Fig. 3(j), depicts the activity of the immune effector being activated by the presence of the virus with smooth convex inclination leading to build-up of

the immune system i.e.  $0.1 \leq E_i(t) \leq 8.87$  cells/ml<sup>3</sup> for all  $t_f \leq 30$  days.

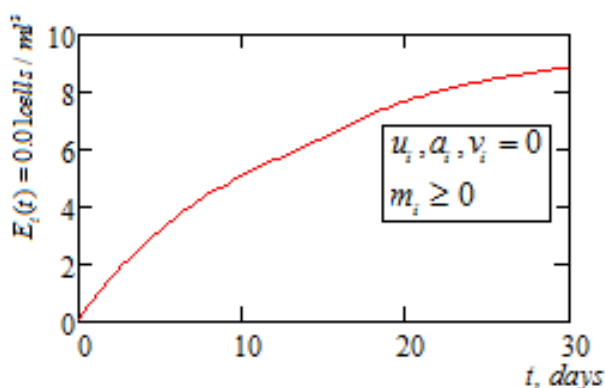


Fig 3(j): Immune effectors under COVID -19 dynamics with off-treatment and  $\mathfrak{R}_{(0)} = 10.159 > 1$

Fig 3 (a-j): Graphical images of computed off – treatment of COVID-19 infection dynamics with  $\mathfrak{R}_{(0)} \cong 10.159 > 1$ .

**5.3. Numerical computation for COVID-19 endemic infection under triple-bilinear controls  $u_i, a_i, v_i > 0$  with  $m_i \geq 0$**

The implementation of the theoretical predictions for the derived system global stability analysis of model (1) is numerically illustrated, following the introduction of designated triple-bilinear control functions: bilinear nonpharmaceutical (face-masking and social distancing), bilinear pharmacotherapy (hydroxylchloroquine - HCQ and azithromycin – AZT) and bilinear immunity controls

(adaptive immune response and **BNT162b2** – vaccines) at specified stages of infection progressions as depicted in Fig. 4(a-j), below. The computation that leads to the following graphical images are in Appendix B1 and B2.

Following the introduction of varying designated treatment functions, we observe from Fig. 4(a), a smooth geometric concave-like surges of the susceptible compartment with value in the range of  $0.5 \leq S_p(t) \leq 91.99$  cells/ml<sup>3</sup> for all  $0 \leq t_f \leq 30$  days.

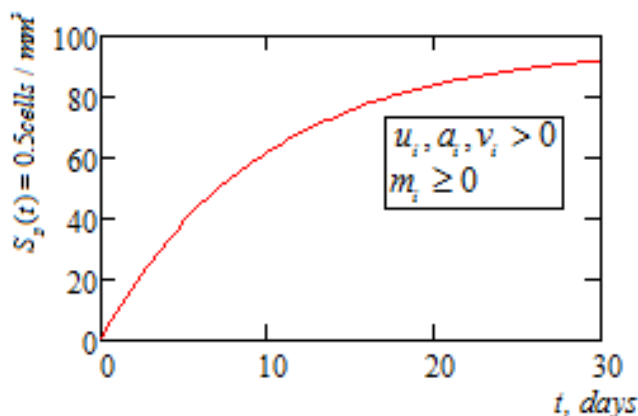


Fig 4(a): Susceptible popn under COVID -19 dynamics with onset-treatment and  $\mathfrak{R}_{0(2)} = -3.01 < 1$

With the introduction of nonpharmaceutical into the exposed compartment, Fig. 4(b), shows a significant reduction in the rate of spread of the virus i.e.  $0.02 \leq X_p(t) \leq 0.3 \text{ cells} / \text{ml}^3$  at the early time

interval of  $0 \leq t_f \leq 8$  days. Thereafter, the exposed population is seen depleting to asymptotic stability with value of  $X_p(t) \leq -1.988 \times 10^{-3} \text{ cells} / \text{ml}^3$  at  $10 \leq t_f \leq 30$  days.

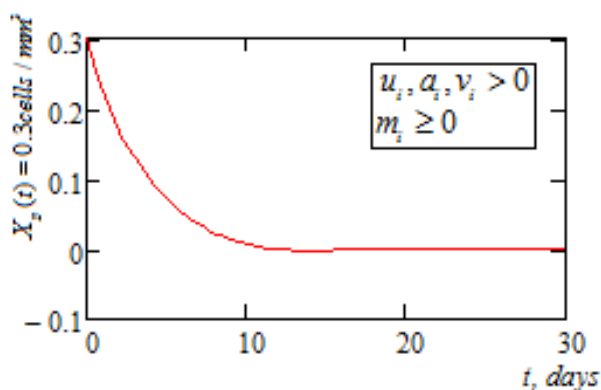


Fig 4(b): Exposed popn under COVID -19 dynamics with onset-treatment and  $\mathfrak{R}_{0(2)} = -3.01 < 1$

From Fig 4(c), we observe the consequential administration of bilinear nonpharmaceutical and vaccination of the susceptible compartment coupled to boasted immune response. This leads to a drastic

reduction of the spread of the virus with declining tail value of  $-2.715 \geq A_u(t) \geq 0.107 \text{ cells} / \text{ml}^3$  for all  $12 \leq t_f \leq 30$  days.

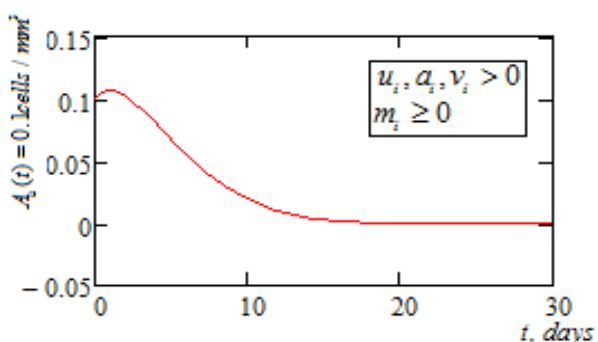


Fig 4(c): Unaware infectives under COVID -19 dynamics with onset-treatment and  $\mathfrak{R}_{0(2)} = -3.01 < 1$

The aware the infective compartments of Fig 4(d), depicting the presence of triple-bilinear control functions coupled to the awareness status, leading to rapid elimination of the virus to an insignificant level

with decline value of  $0.15 \geq I_a(t) \geq 4.598 \times 10^{-8} \text{ cells} / \text{ml}^3$  for all  $14 \leq t_f \leq 30$  days.

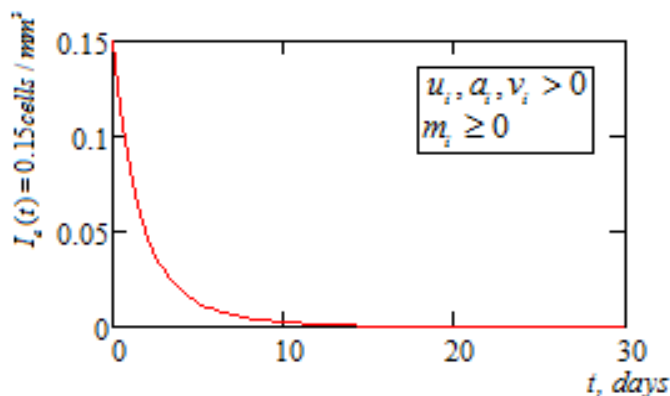


Fig 4(d): Aware infectives under COVID -19 dynamics with onset-treatment and  $\mathfrak{R}_{0(2)} = -3.01 < 1$

Fig 4(e), depicts the isolated compartment, where patients are under intensive care. The vaccination of the compartments, which also boasts adaptive immune effectors, lead to rapid smooth concave-like

declination and elimination of the virus with value  $0.03 \geq I_s(t) \geq 3.472 \times 10^{-6} \text{ cells/ml}^3$  for all  $0 \leq t_f \leq 20$  days.

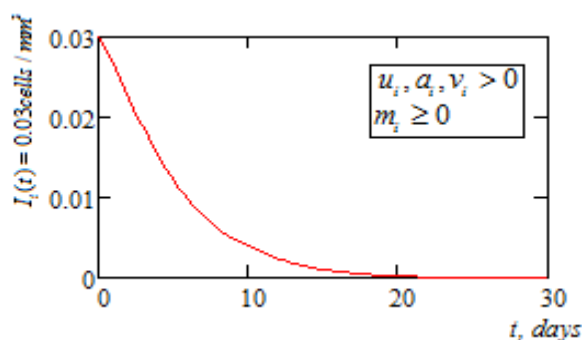


Fig 4(e): Isolated infectives under COVID -19 dynamics with onset-treatment and  $\mathfrak{R}_{0(2)} = -3.01 < 1$

Fig 4(f), represents super-spreader compartment, where under triple-bilinear control. Under this condition, the population of super-spreaders are under check declining with concave-like smooth

curve and tailings to zero stability with value range of  $0.052 \geq S_s(t) \geq -8.547 \times 10^{-8} \text{ cells/ml}^3$  for all  $0 \leq t_f \leq 30$  days.

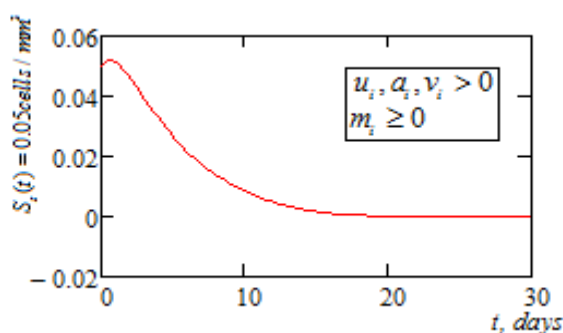


Fig 4(f): Super-spreaders under COVID -19 dynamics with onset-treatment and  $\mathfrak{R}_{0(2)} = -3.01 < 1$

Under triple-bilinear control function, the initial influx of the infected population to the hospital in the first-three days with value at  $0 \leq H_i(t) \leq 0.013 \text{ cells/ml}^3$  for all  $0 \leq t_f \leq 3$  days, as in Fig. 4(g), is seen

to sharply decline at  $3 \leq t_f \leq 20$  days and then after, terminate to near zero for all  $20 \leq t_f \leq 30$  days.

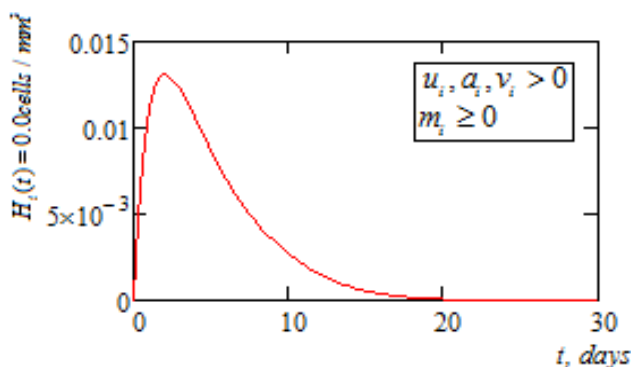


Fig 4(g): Hospitalized infectives under COVID -19 dynamics with onset-treatment and  $\mathfrak{R}_{0(2)} = -3.01 < 1$

From Fig 4(h), we observe that the reservoir of aerosol viral load exhibited a docilely incline undulating curve at  $0 \leq t_f \leq 20$  days and then attaining

near stability after  $20 \leq t_f \leq 30$  days, with value at  $0.025 \leq C_v(t) \leq 2.738$ .

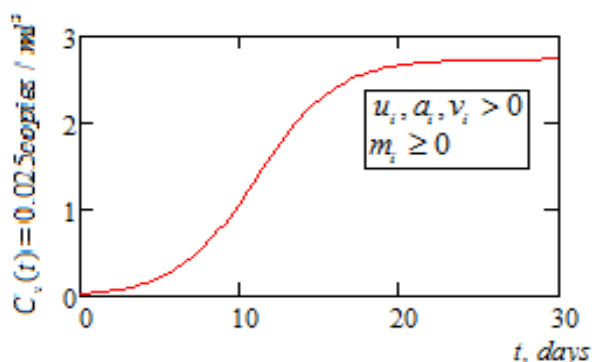


Fig 4(h): Aerosol infectious virions dynamics with onset-treatment and  $\beta_i(\hat{N}) = -3.379 \times 10^{-5}$

We observe from Fig 4(i), the access to multiple control functions leads to massive recovery. That is, the compartment exhibits a concave-like

smooth inclination with value range of  $0 \leq R_p(t) \leq 7.818 \text{ cells} / \text{ml}^3$  for all  $0 \leq t_f \leq 30$  days.

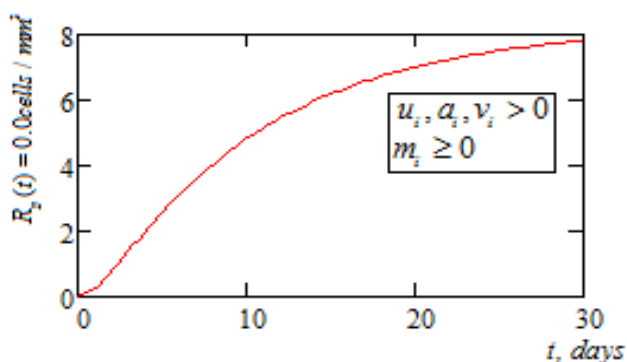


Fig 4(i): Recover infectives under COVID -19 dynamics with onset-treatment and  $\mathfrak{R}_{0(2)} = -3.01 < 1$

The manifestation of the recovery compartment is vindicated by the smooth concave-like inclination of the adaptive immune effector, which is attributive to induce vaccination, leading to build-up of

the adaptive immune effectors with value at  $0.1 \leq E_i(t) \leq 7.607 \text{ cells} / \text{ml}^3$  for all  $0 \leq t_f \leq 30$  days as depicted by Fig. 4(j).

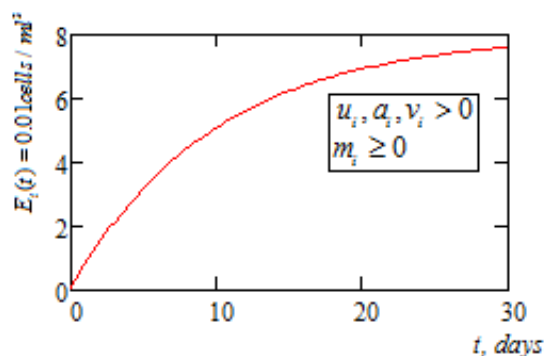


Fig 4(j): Immune effectors under COVID -19 dynamics with onset-treatment and  $\mathfrak{R}_{0(2)} = -3.01 < 1$

**Fig 4 (a-j): Graphical images of computed onset – treatment of COVID-19 infection dynamics with  $\mathfrak{R}_{0(2)} \cong -3.01 < 1$**

### 6. DISCUSSION OF RESULTS

Motivated by the limitation of a foregoing leading paper, an 8-Dimensional mathematical model for COVID-19 pandemic was formulated and studied [2]. In that study, the following were noted: the adverse ingress rate of aerosol infectious virions was not considered; the potent of adaptive immune effectors as well as non-introduction of vaccination at community level were completely avoided. Moreover, ignored was the potential role of system immune delay lag. Ignited by these surmountable clinical overviews, the present study exploring global stability theory, sought and projected an improved deterministic COVID-19 mathematical dynamic modeled saddle with the task of evolving optimal treatment strategy that maximizes not only the healthy susceptible community but also, enhanced immune effector cells. With the incorporation of aerosol virus dynamic flow and the biological impact of adaptive immune effectors, the system was analyzed based on 10-subpopulation and investigated following the introduction of vaccines in the presence of dual bilinear control functions. That is, on account of the dual role of adaptive immune effectors as both state-space and control function, the control functions with the acronym “triple-bilinear” control measures include: bilinear nonpharmaceutical (face-masking and social distancing), bilinear pharmacotherapy (hydroxylchloroquine - HCQ and azithromycin – AZT) and bilinear immunity controls (adaptive immune response and **BNT162b2** – vaccines) were administered at varying designated stages.

The predominant assumption of the study were the accommodation of system immunity delay lag and the introduction of the vaccine in susceptible and isolated communities. Moreso, apart from the application of the fundamental theory of differential equations for the verification of model well-posedness, the material and methods of the study further explored classical method of Lyapunov functions with the incorporation of the theory of Volterra-Lyapunov stable matrices for the analysis of system global stability conditions. Furthermore, the study was investigated for

both untreated and onset – treatment of endemic scenarios and numerical computations conducted using in-built Runge-Kutta of order of precision 4 in a Mathcad surrounding. Vital to the study is the potential role of the system basic reproduction number. Thus, the reproduction numbers for both off/onset treatments were simulated accordingly.

From the computations of the system basic and effective reproduction number, the results as in Fig. 2(a-b) shows that for off-treatment scenario, the basic reproduction number was computed as  $\mathfrak{R}_{0(1)} \cong 10.159 > 1$ , which explicitly conformed to the findings ( $\mathfrak{R}_{0(1)} = 10.94$ ) from [2]. Notable and significant variation is observed from the improved value obtained for the onset-treatment of the present study ( $\mathfrak{R}_{0(2)} \cong -3.01 < 1$ ) as against that of our motivated model with  $\mathfrak{R}_{0(2)} = 3.224$ . Of note, this great achievement can be attributed to the incorporation of third bilinear control functions (the role of adaptive immune response and **BNT162b2** – vaccine) and the constructive biological inclusion of immunity delay lag, as was clearly noted by the study assumptions.

Further simulations as in Fig. 3(a-j) indicated that given an off-treatment scenario, the force of infection depicted by  $\beta_i(\hat{N}) = 1.69 \times 10^{-4}$  represent dose of heavy droplets of aerosol viral load of COVID-19 that will conveniently contaminate upon contact, a proportion of susceptible population  $S_p(t) \leq 67.132 \text{ cells} / \text{ml}^3$  with average reproduction number of  $\mathfrak{R}_{0(1)} = 10.159 > 1$  within the first-twelve days ( $t_f \leq 12$  days) of asymptomatic stage of infection. This asymptomatic period agrees with the established viral load incubation period of 2 – 14 days for COVID-19, [4,5]. Moreso, the result under off-treatment scenario is in agreement with the findings [2]. Moreover noted here there is the significant variation of the computed force of infection with value at  $\beta_i(\hat{N}) = 2.12 \times 10^{11}$ , [2] as against the present value of

$\beta_i(\hat{N}) = 1.69 \times 10^{-4}$ . This present result could be attributed to the introduction of two major components: system immunity lag and the adaptive immune effectors at the onset of infection. Clearly, after the asymptotic stages, which signifies the incubation period, the susceptible population is seen to rapidly decline following the manifestation of the symptomatic stage of the infection leading to contamination of the susceptible population with surviving proportion of  $S_p(t) \leq 0.5 \text{ cells/ml}^3$ , which is known to emanates from the existing natural recruitment rate  $b_p = 0.5 \text{ cells/ml}^3$  for all  $14 \leq t_f \leq 30$  days.

Notably, under off-treatment scenario, as depicted by Fig. 3(a-j), it was noted that at the asymptomatic stage of the infection, the susceptible populations were seen growing (see Fig. 3(a)), while varying infection rates were insignificant as a portrait by Fig 3(a-d, f-i). These results explicitly confirm the exponential transmissibility of the virus at incubation period of 2–14 days and firmly agreed with established fact that sample collection for testing should be obtained within the first – ten days of first contact with the virus, [36]. Isolated population completely extinguished after  $t_f \leq 10$  days (see Fig. 3(e)). The concentrations of aerosol viral load remain high after  $t_f \leq 10$  days with value at  $0 \leq C_v(t) \leq 6.152$  for all  $18 \leq t_f \leq 30$  days. Fig. 3(j) buttresses the fact that the presence of virus causes an intensive build-up of adaptive immune effectors with value  $0 \leq E_i(t) \leq 8.87 \text{ cells/ml}^3$  for all  $t_f \leq 30$  days.

With the introduction of triple-bilinear control at varying designated stages, it was observed that recovery and the susceptible populations exhibited proportionate geometric rejuvenation with respective values at  $(0 \leq R_p(t) \leq 7.818$  and  $0.5 \leq S_p(t) \leq 91.991)$   $\text{cells/ml}^3$  for all  $0 \leq t_f \leq 30$  days – see Figs 4(j) and (a). These results are an improvement against the corresponding off-treatment scenario and when compared to the onset-treatment scenario of the model [2]. Moreso, the application of early onset treatment saw near total eradication of infection in the aware infective compartment within the first-fourteen days i.e.  $0.15 \geq I_a(t) \geq 4.598 \times 10^{-8} \text{ cells/ml}^3$  for all  $14 \leq t_f \leq 30$  days, while both exposed class unaware infectives and super-spreaders indicated near complete eradication with values at  $(X_p(t) \leq -1.988 \times 10^{-3}$ ,  $A_u(t) \leq -2.71$  and  $S_s(t) \leq -8.547 \times 10^{-8}) \text{ cells/ml}^3$  for all  $10 \leq t_f \leq 30$  days respectively. Infection of both isolated and hospitalization compartments depicted near complete eradication of the virus with persisting insignificant values of  $(I_s(t) \leq 3.472 \times 10^{-6}$  and

$H_i(t) \geq 0) \text{ cells/ml}^3$  for all  $0 \leq t_f \leq 20$  days. This result further agrees with system theoretical predictions where following introduction of designated control functions, the pandemic curves clearly exhibited intrinsically stable dynamical system.

Remarkably, the concentrated aerosol viral load with inclined value of  $0.025 \leq C_v(t) \leq 2.738$  as depicted by Fig. 4(h) clearly affirmed the lack of complete eradication of the virus within the system. Rather, like most other transmittable diseases, its portrait the persistence of the virus within the environment but could be docile provided communities adhered to the aforementioned methodological control measures. Furthermore, the persistence of aerosol viral load and induced vaccination clearly leads to the biological rebuild of the adaptive immune effectors, potent to counter reemergence of the virus – see Fig. 4(j). Finally, for a more in-depth appreciation of the current study, we present, as in appendix C, a summary of the comparison of the results of onset-treatments of the present study and that of our motivating model [2].

## 7. CONCLUSION

Following the availability of vaccines for the inhibition of the dreaded COVID-19, and triggered by the non-availability of coinciding mathematical models for the epidemiological analyses of the treatment and control of COVID-19 via multi-combination of control measures and coupled with the lack of explicit derivation of COVID-19 reproduction number for both off-treatment  $\mathfrak{R}_{0(1)}$  and onset-treatment  $\mathfrak{R}_{0(2)}$  scenarios, the present study sought and presented an expanded 10-Dimensional deterministic COVID-19 dynamic model that accounted for the role of triple-bilinear control functions for the treatment of COVID-19 in Nigeria. The interactions between the vector and the subpopulations adopted the hypo-to-hyper transmission mode.

The study was triggered with the problem statement followed by the derivation of the model equations and then the investigation of the mathematical properties following thereof. Both the system force of infection  $\beta_i(\hat{N})$  and the reproduction number ( $\mathfrak{R}_0$ ) for both off-treatment  $\mathfrak{R}_{0(1)}$  and onset-treatment  $\mathfrak{R}_{0(2)}$  scenarios was for the first-time, determined and computed. We analyze the model local and endemic stability in terms of system reproduction number and thereafter, explored the method of Lyapunov functions in conjunction with Volterra-Lyapunov stable matrix to investigate the global stability conditions for the derived COVID-19 model and studied under triple-bilinear control protocol. The theoretical predictions indicated that COVID-19 free equilibrium and its endemic equilibrium were both locally and globally asymptotically stable for all

$\mathfrak{R}_0 < 1$  as vindicated by computed  $\mathfrak{R}_{0(2)} \cong -3.01 < 1$ .

Further numerical results showed that for off-treatment scenario, the system exhibited asymptomatic early infection within the first 12 days, which not only affirmed the exponential spread of the virus within its incubation period of 2–14 days but further strengthen the suggestion for collection of an active samples for testing within the first ten days of infection. Moreso, it was observed that rapid extinction of the susceptible population occurred after 14 days, leading to exponential spread of the virus as depicted by the varying infectious compartments.

None-less, the introduction of triple-bilinear control function at designated compartments saw enhanced rejuvenation of susceptible and recovered as well as a massive build-up of adaptive immune effectors, which signified the ingenuity and compatibility of the model to real-life situations. That is, numerical results further agree with system theoretical predictions with curves clearly exhibiting intrinsically stable dynamical system. Moreso, the rapid near-zero eradication of the virus within the first fourteen days dignified the superiority of triple-bilinear control approach to dual-bilinear technique, where infection although reduced but persisted higher [2]. Furthermore, the investigation also revealed that while the spread and infection dynamics could be curtailed to near zero threshold, the reservoir (environment) of COVID-19 viral load could persist but docile provided the prescribed triple-bilinear controls are coherently adhered by the population. Thus, in reality, this finding will be of immense benefit to both government and non-governmental agencies in decision and policy making towards sustaining the near-zero eradication of the dreaded COVID-19 pandemic in Nigeria and possibly beyond. Therefore, it is suggested that for a possible complete zero eradication of the virus, the application of the optimal control technique will be highly ascribed.

#### Data availability

The data generated for this mathematical modeling include those obtained from UCTH – Calabar and Cross River State Ministry of Health, in affiliation with published parameter values and are accordingly cited.

#### Funding and acknowledgement

This research, which covers the Phase –II (final) of the research grant, is funded by TETFund – IBR in conjunction with University of Cross River State – (Unicross), under the project *TETF/DR&D/CE/UNI/CAL/RG/2021/Vol.1*. The authors are indeed appreciative of the support from TETFund, Cross River State Ministry of Health and the University of Calabar Teaching Hospital – UCTH, Calabar, for access to their records for this project.

#### Declaration of competing interest

The corresponding author on behalf of the authors attest to the fact that there exists no conflict of interest in the submission of this manuscript and that the entire content remains the original recipes of the authors, which had not been submitted for consideration to any journal outfit.

#### Credit authorship contribution statement

The authors' contributions to this manuscript were thus - **Bassey Echeng Bassey**: conceptualization, methodology, data collections, writing – original draft, writing – reviews and editing, algorithm and software programing, analysis and writing of final version. **Igwe O. Ewona**: Methodology, supervision, formal analysis, editing and valuations

#### REFERENCES

- Gumel, A. B. (2020). Using mathematics to understand and control the coronavirus pandemic. Retrieved date: [15, May, 2022], online available at <https://opinion.premiumtimesng.com/2020/05/04/using-mathematics-to-understand-and-control-the-coronavirus-pandemic-by-abba-b-gumel/>.
- Bassey, E. B., & Atsu, U. J. (2021). Global stability analysis of the role of multi-therapies and non-pharmaceutical treatment protocols for COVID-19 pandemic. *Chaos, Solitons and Fractals*, 143(2021), 110574. <https://pubmed.ncbi.nlm.nih.gov/33519116/> or at: <https://www.sciencedirect.com/science/article/abs/pii/S0960077920309656?via%3Dihub>
- Bekker, L., & Mizrahi, V. (2020) COVID-19 research in Africa. Retrieved date: [29, August, 2021], online available at: <http://science.sciencemag.org/content/368/6494/919>
- Leslie, M. (2020). T cells found in coronavirus patients 'bode well' for long-term immunity. Retrieved date: [14, August, 2021], online available at <http://science.sciencemag.org/content/368/6493/809>
- Grigorieva, E., Khailov, E., & Korobeinikov, A. (2020). Optimal quarantine strategies for COVID-19 control models. Retrieved date: [29, August, 2021], online available at <https://arxiv.org/pdf/2004.10614.pdf>
- Altan, A., & Karasu, S. (2020). Recognition of COVID-19 disease from X-ray images by hybrid model consisting of 2D curvelet transform, chaotic salp swarm algorithm and deep learning technique. *Chaos, Solitons and Fractals*, 140(2020), 110071, 1-10.
- Yang, W., & Yan, F. (2020). Patients with RT-PCR confirmed COVID-19 and normal chest CT. *Radiology*, 2020, 200702.
- Alhumaid, K., Sana Ali, S., Waheed, A., Zahid, E., & Habes, M. (2020). COVID-19 & e-learning: perceptions & attitudes of teachers towards e-

- learning acceptance in the developing countries. *Multicultural Education*, 6(2), 100-115.
9. WHO. (2021). Evaluation of COVID-19 vaccine effectiveness. Retrieved date: [04, May, 2022], online Available at [https://www.who.int/publications/i/item/WHO-2019-nCoV-vaccine\\_effectiveness-measurement-2021.1](https://www.who.int/publications/i/item/WHO-2019-nCoV-vaccine_effectiveness-measurement-2021.1)
  10. Duška, F., Waldauf, P., Halačová, M., Zvoniček, V., Bala, J., Balík, M., ... & Černý, V. (2020). Azithromycin added to hydroxychloroquine for patients admitted to intensive care due to coronavirus disease 2019 (COVID-19)—protocol of randomised controlled trial AZIQUINE-ICU. *Trials*, 21(1), 1-11. Retrieved date: [14, July, 2022], online Available at <https://www.researchsquare.com/article/rs-22892/v2>
  11. Gumel, A. B., Iboi, E. A., & Ngonghala, C. N. (2020). Will an imperfect vaccine curtail the COVID-19 pandemic in the U.S.? *Infectious Disease Modelling*, 5(2020), 510-524.
  12. Feng, G., Zhang, L., Wang, K., Chen, B., & Hua-Xiang Xia, H. (2021) Research, Development and Application of COVID-19 Vaccines: Progress, Challenges, and Prospects. *Journal of Exploratory Research in Pharmacology*, 6(2), 31–43.
  13. Alqudeimat, Y., Alenezi, D., AlHajri, B., Alfouzan, H., Almokhaizeem, Z., Altamimi, S., ... & Ziyab, A. H. (2021). Acceptance of a COVID-19 vaccine and its related determinants among the general adult population in Kuwait. *Medical Principles and Practice*, 30(3), 262-271.
  14. Antonelli, M., Penfold, R. S., Merino, J., Sudre, C. H., Molteni, E., Berry, S., ... & Steves, C. J. (2022). Risk factors and disease profile of post-vaccination SARS-CoV-2 infection in UK users of the COVID Symptom Study app: a prospective, community-based, nested, case-control study. *The Lancet Infectious Diseases*, 22(1), 43-55.
  15. Wahid, B. K. A., Moustapha, D., Rabi, H. G., & Bisso, S. (2020) Contribution to the Mathematical Modeling of COVID-19 in Niger. *Applied Mathematics*, 11, 427-435. Retrieved date: [02, August, 2022], online available at <https://doi.org/10.4236/am.2020.116030>
  16. Hellewell, J., Abbott, S., Gimma, A., Bosse, N. I., Jarvis, C. I., Russell, T. W., ... & Eggo, R. M. (2020). Feasibility of controlling COVID-19 outbreaks by isolation of cases and contacts. *The Lancet Global Health*, 8(4), e488-e496. Retrieved date: [24, August, 2022], online available at [https://www.thelancet.com/article/S2214-109X\(20\)30074-7/fulltext](https://www.thelancet.com/article/S2214-109X(20)30074-7/fulltext)
  17. Kucharski, A. J., Russell, T. W., Diamond, C., Liu, Y., Edmunds, J., Funk, S., ... & Flasche, S. (2020). Early dynamics of transmission and control of COVID-19: a mathematical modelling study. *The lancet infectious diseases*, 20(5), 553-558. Retrieved date: [24, July, 2022], online available at <https://www.ncbi.nlm.nih.gov/pmc/articles/PMC7158569/>
  18. Liu, Y, Gayle, A. A., Wilder-Smith, A., & Rocklöv, J. (2020). The reproductive number of COVID-19 is higher compared to SARS coronavirus. *J. Travel Med*, 1–4. doi: 10.1093/jtm/taaa021. Retrieved date: [06, August, 2022], online available at <https://pubmed.ncbi.nlm.nih.gov/32052846/>
  19. Torres, D. F. M., Ndairou, F., Area, I., & Nieto, J. J. (2020). Mathematical modeling of COVID-19 transmission dynamics with a case study of Wuhan. *Chaos, Solitons and Fractals*. Retrieved date: [02, August, 2022], online available at <http://ees.elsevier.com>
  20. Iboi, A. E., Ngonghala, C., & Gumel, A. B. (2020). Will an imperfect vaccine curtail the COVID-19 pandemic in the U.S.? *Journal of Infectious Disease Modelling*, 5, 510-524.
  21. Zhu, N., Zhang, D., Wang, W., Li, X., Yang, B., & Song, J. (2019) A novel coronavirus from patients with pneumonia in China. *N Eng J Med*, 382, 727–33, online available at <https://doi.org/10.1056/NEJMoa2001017>.
  22. Adams, B. M., Banks, H. T., Hee-Dae, K., & Tran, H. T. (2004). Dynamic Multidrug Therapies for HIV: Optimal and STI Control Approaches. Retrieved date: [24, July, 2022], online available at <http://citeseerx.ist.psu.edu/viewdoc/summary?doi=10.1.1.400.9056>
  23. Ezegu, N. J., Togbenon, H. A., & Moyo, E. (2019). Modeling and analysis of cholera dynamics with vaccination. *American Journal of Applied Mathematics and Statistics*, 7(1), 1-8.
  24. Edward, S., & Nyerere, N. (2015). A mathematical model for the dynamics of cholera with control measures. *Applied and Computational Mathematics*, 4(2), 53-63.
  25. Hattaf, K., & Yousfi, N. (2018) Modeling the adaptive immunity and both modes of transmission in HIV infection. *Computation*, 6(37), 1-18.
  26. Osman, S., Makinde, O. D., & Theuri, D. M. (2018). Stability analysis and modeling of listeriosis dynamics in human and animal populations. *Global Journal of Pure and Applied Mathematics*, 14(1), 115-138.
  27. Diekmann, O., Heesterbeek, J. A. P., & Metz, J. A. J. (1990). On the definition and the computation of the basic reproduction ratio  $R_0$  in models for infectious diseases in heterogeneous populations. *J Math Biol*, 28(1990), 365-368.
  28. Van den Driessche, P., & Watmough, J. (2002). Reproduction numbers and sub-threshold endemic equilibria for compartmental models of disease transmission. *Mathematical Biosciences*, 180(2002), 29–48.
  29. Kahuru, J., Luboobi, L., & Nkansah-Gyekye, Y. (2017a). Stability analysis of the dynamics of tungiasis transmission in endemic areas. *Asian*

- Journal of Mathematics and Applications*, 2017, 1-24.
30. Zahedi, M. S., & Kargar, N. S. (2017). The Volterra-Lyapunov matrix theory for global stability analysis of a model of the HIV/AIDS. *Int J Biomath*, 10(1), 1-21.
  31. Bassey, E. B. (2020). Dynamic Optimal Control for Multi-chemotherapy Treatment of Dual Listeriosis Infection in Human and Animal Population. *Applications and Applied Mathematics: An International Journal*, 15(1), 192–225. online available at <http://pvamu.edu/aam>
  32. Wang, M., Cao, R., Zhang, L., Yang, X., Liu, J., Xu, M., ... & Xiao, G. (2020). Remdesivir and chloroquine effectively inhibit the recently emerged novel coronavirus (2019-nCoV) in vitro. *Cell research*, 30(3), 269-271.
  33. Castillo-Chavez C, Feng Z., & Huang W. (2002). On the computation of  $R_0$  and its role on global stability in mathematical approaches for emerging and re-emerging infectious disease: an introduction. *IMA Volumes in Math Approaches*, 125, 229–50. online available at <https://ecommons.cornell.edu/bitstream/handle/1813/32146/BU-1553-M.pdf?sequence=1>.
  34. Lyapunov, A. M. (1992). The General Problem of the Stability of motion, (A. T. Fuller trans.) *Taylor and Francis*, London.
  35. Bassey, E. B., & Adagba, O. H. (2021). Global stability analysis of the role of antiretroviral therapy (ART) abuse in HIV/AIDS treatment dynamics. *Pure and Applied Mathematics Journal*, 10(1), 9-31, doi: 10.11648/j.pamj.20211001.12.
  36. World Health Organization. (2020). Coronavirus disease 2019 (covid-19): situation report, 51. Geneva: World Health Organization. Online retrieve, [May 26, 2021]. Available at: <https://apps.who.int/iris/handle/10665/331475>
  37. Bassey, E. B., & Igwe, O. E. (2022). On determinism, well-posedness and the application of Cauchy-Lipschitz conditions for a hypo-hyper covid-19 epidemic model. *Unicross Journal of Science and Technology – UJOST*, 1(2), 93-110.
  38. Tutsoy, O., & Tanrikulu, M. Y. (2022). Priority and age specific vaccination algorithm for the pandemic diseases: a comprehensive parametric prediction model. *BMC Medical Informatics and Decision Making*, 22(1), 1-12.
  39. Fleming, W. H., & Rishel, R. W. (2012). *Deterministic and stochastic optimal control* (Vol. 1). Springer Science & Business Media.
  40. Fleming, W. H., & Rishel, R. W. (2012). *Deterministic and Stochastic Optimal Control*// Springer, 1975. Verlag, New York.
  41. Joshi, H. R. (2002). Optimal control of an HIV immunology model. *Optimal control applications and methods*, 23(4), 199-213.